Lifetime of the first and second collective excitations in metallic nanoparticles

Guillaume Weick, Rafael A. Molina, Dietmar Weinmann, Rodolfo A. Jalabert

Lifetime of the first and second collective excitations in metallic nanoparticles

Guillaume Weick,[1,2,*] Rafael A. Molina,[3] Dietmar Weinmann,[1] and Rodolfo A. Jalabert[1]

[1] *Institut de Physique et Chimie des Matériaux de Strasbourg, UMR 7504 (ULP-CNRS), BP 43, F-67034 Strasbourg Cedex 2, France*
[2] *Institut für Physik, Universität Augsburg, D-86135 Augsburg, Germany*
[3] *Max-Planck-Institut für Physik komplexer Systeme, D-01187 Dresden, Germany*

(Dated: September 12, 2005)

We determine the lifetime of the surface plasmon in metallic nanoparticles under various conditions, concentrating on the Landau damping, which is the dominant mechanism for intermediate-size particles. Besides the main contribution to the lifetime, which smoothly increases with the size of the particle, our semiclassical evaluation yields an additional oscillating component. For the case of noble metal particles embedded in a dielectric medium, it is crucial to consider the details of the electronic confinement; we show that in this case the lifetime is determined by the shape of the self-consistent potential near the surface. Strong enough perturbations may lead to the second collective excitation of the electronic system. We study its lifetime, which is limited by two decay channels: Landau damping and ionization. We determine the size dependence of both contributions and show that the second collective excitation remains as a well-defined resonance.

PACS numbers: 78.67.Bf, 73.20.Mf, 71.45.Gm, 31.15.Gy

I. INTRODUCTION

The surface plasmon (SP) resonance is a very important collective excitation in metallic clusters.[1,2] It is the dipolar vibration of the electronic center of mass with respect to the positive ionic charge, analogous to the giant resonance of nuclei.[3] Since an external electromagnetic dipole field couples directly to the electronic center of mass, the photoabsorption spectrum of a metallic cluster is dominated by the SP. The lifetime of this collective excitation is a determining factor in the relaxation process studied in femtosecond pump-probe experiments.[4]

The classical electromagnetic theory for a charged metallic sphere in the vacuum yields the energy $\hbar\omega_{\rm M}$ of the resonance, with the Mie frequency $\omega_{\rm M} = \omega_{\rm p}/\sqrt{3}$, where $\omega_{\rm p} = (4\pi n e^2/m_{\rm e})^{1/2}$ is the bulk plasma frequency of the metal, n, e, and $m_{\rm e}$ being the electron density, charge, and mass, respectively. If the clusters are embedded in a matrix (of dielectric constant $\epsilon_{\rm m}$) and/or we consider noble metal clusters (where the effect of the d electrons can be modeled by a dielectric function $\epsilon_{\rm d}$) the Mie frequency takes the form $\omega_{\rm M} = \omega_{\rm p}/\sqrt{\epsilon_{\rm d} + 2\epsilon_{\rm m}}$. The Mie frequency is close to the experimentally measured resonances. Such an agreement is not surprising since we deal with a collective excitation with a clear classical counterpart. Small red- and blueshifts with respect to $\omega_{\rm M}$ have been experimentally observed in different physical conditions, and various microscopic approaches have been developed to account for the frequency shifts.[1,2] The most successful among them are based on a jellium description (where the ionic positive charges are taken as a uniform background) and linear-response theory in the framework of the time-dependent local density approximation (TDLDA).[5]

While it is difficult to measure the SP lifetime, numerous data for the linewidths of the absorption peak of ensembles of nanoparticles are available,[1,2,6,7] but their theoretical analysis has proven to be quite involved. In principle, inhomogeneous effects arising from the dispersion among the probed ensemble of clusters have to be separated from the properties of single particles. Intrinsic effects depending on the bulk properties of the metal have to be separated from size-dependent properties of the cluster, and from the effect of the interaction with the local environment (matrix). In addition, the decay of the SP may follow different channels depending on the size of the cluster.[2] We calculate the Landau damping contribution to the linewidth (i.e. decay into particle-hole pairs), which dominates in the case of small clusters of radius a in the range 0.5–2.5 nm.[3] For larger particles the Landau damping competes with radiation damping.

Recent measurements of single-cluster optical absorption have rendered accessible the optical properties of individual nano-objects.[8,9,10] Most of the individual nanoparticles studied so far (in static[8] or dynamic[9] setups) are too large to be in the Landau regime. However the linewidth of a single 2.5 nm radius gold nanoparticle has been determined lately.[10] The possibility of overcoming the inhomogeneous broadening, and the application as biological markers, resulted in a renewed interest for the optical response of metallic clusters.

Kawabata and Kubo studied the Landau damping of the SP,[11] and using linear response theory they proposed a total linewidth

$$\Gamma_{\rm t}(a) = \Gamma_{\rm i} + \Gamma(a),$$

with $\Gamma_{\rm i}$ a constant intrinsic width and $\Gamma(a)$ inversely proportional to the particle size a. Barma and Subrahmanyam,[12] and Yannouleas and Broglia[13] improved this calculation and proposed corrections to the behavior of Γ outside the regime $\hbar\omega_{\rm M}/\varepsilon_{\rm F} \ll 1$, where $\varepsilon_{\rm F}$ is the Fermi energy. They obtained

$$\Gamma(a) = \frac{3}{2}\frac{\varepsilon_{\rm F}}{k_{\rm F}a} g(\xi), \qquad (1)$$

where $k_{\rm F}$ is the Fermi wave-vector, and g a function of the ratio $\xi = \hbar\omega_{\rm M}/\varepsilon_{\rm F}$. Numerical calculations within the TDLDA on free alkaline clusters[14] agree with this analytical result for $1.5 \leqslant a \leqslant 2.5$ nm. For smaller radii, Γ shows a nonmonotonous size dependence superposed to the overall behavior of Eq. (1). These shell effects arise from the electron-hole density-density correlations in the angular-momentum restricted density of states,[15] and a semiclassical evaluation of Γ is in good agreement with TDLDA calculations.

The experimentally observed nonmonotonous size dependence of the plasmon linewidth for charged alkaline metal nanoparticles in vacuum[6] is consistent with the theoretical calculations. However, our calculated linewidths yield lower bounds for the experimentally measured ones, and the corresponding lifetimes are upper bounds of those found in real systems. Further measurements with smaller radii and a narrower size-distribution seem necessary to clearly establish the connection with the theory.

Noble metal clusters embedded in inert matrices[7] also exhibit a nonmonotonous linewidth for small a. However, a direct application of Eq. (1) overestimates the smooth part of Γ.[15] This discrepancy motivates us to develop a refined theoretical description of the SP lifetime for the case of clusters with internal dielectric constant $\epsilon_{\rm d}$ and surrounded by a dielectric medium with constant $\epsilon_{\rm m}$. The presence of an inhomogeneous dielectric environment leads to the modification of Eq. (1).

Under a weak initial optical excitation, only the first surface plasmon (that we simply denote "surface plasmon" when there is no possibility of confusion) is excited. With sufficiently strong initial excitations, we can also reach the second quantum level of the center-of-mass motion, known as the second (or double) plasmon. Such a resonance will be experimentally relevant provided its lifetime is sufficiently large (in the scale of $\omega_{\rm M}^{-1}$). The lifetime is given by the anharmonicities of the center-of-mass system and by its interactions with the other degrees of freedom. Like in the previous discussion, the Landau damping is an important channel for the decay of the second plasmon, but a new channel appears when $2\hbar\omega_{\rm M}$ is larger than the ionization energy: the ionization in which the cluster looses an electron into the continuum.[16] Such a process was discussed in order to interpret the ionization of charged Na_{93}^{+} clusters observed by Schlipper and collaborators.[17]

We calculate the decay rates associated with different channels for the single- and double-plasmon states using a semiclassical approach within a mean-field description of the nanoparticle. Whenever it is possible, we verify the semiclassical approach by comparing to numerical calculations. We characterize the size-dependent oscillations of the first and second plasmon linewidths for the case of free alkaline metals. In addition, we analyze the theoretical difficulties in extending these calculations to the case of embedded and/or noble metal clusters and propose a way to overcome them. We also apply our semiclassical approach to the calculation of the ionization rate via the double-plasmon channel, and obtain results comparable with the experiments.[17]

The paper is organized as follows: In Sec. II we introduce the basic formalism for the photoabsorption and the SP linewidth. In Sec. III we present the semiclassical calculation of the single-plasmon linewidth, testing some of the approximations that we will use in the sequel. In Sec. IV we study the case of noble metal nanoparticles embedded in a dielectric medium and present the need to improve the existing theory for this case. In Sec. V we show a semiclassical description of the two main channels contributing to the decay of the double plasmon: Landau damping and ionization. Finally in Sec. VI we draw the conclusions and the perspectives of our work. We relegate to the appendix a few technical, but important issues; in Appendix A we extend the standard calculation of the plasmon linewidth to the case where the cluster is made of a noble metal and/or is embedded in a nonreactive matrix. In Appendix B we show how to take advantage of the spherical symmetry in semiclassical calculations like the ones of this paper, and how to recover some well-known results. In Appendix C we present the frequency dependence of the different plasmon linewidths.

II. PHOTOABSORPTION AND PLASMON LINEWIDTH

When the cluster is placed in an electromagnetic field with a wavelength much larger than its size,[18] the photoabsorption cross section is obtained from the application of the dipole operator on the ground state of the system:

$$\sigma(\omega) = \frac{4\pi e^2\omega}{3c}\sum_f |\langle f|z|0\rangle|^2\,\delta(\hbar\omega - E_f), \qquad (2)$$

where c is the velocity of light; $|f\rangle$ and E_f are, respectively, the many-body excited states and eigenenergies of the electronic system. The ground state is noted as $|0\rangle$ and its energy is taken as zero. In Eq. (2), the photon degrees of freedom have already been integrated out. In order to describe the electronic system, we consider a closed shell nanoparticle (perfectly spherical with a "magic number" of atoms) within a jellium model. The Hamiltonian representing N valence electrons in a uniformly positively charged sphere of charge $+Ne$ is given by

$$H = \sum_{i=1}^{N}\left[\frac{p_i^2}{2m_{\rm e}} + U(r_i)\right] + \frac{1}{2}\sum_{\substack{i,j=1\\(i\neq j)}}^{N}\frac{e^2}{|\mathbf{r}_i - \mathbf{r}_j|}, \qquad (3)$$

with the single-particle confining potential

$$U(r) = \begin{cases} 2\pi n e^2\left(\dfrac{r^2}{3} - a^2\right), & r \leqslant a, \\ -4\pi n e^2\dfrac{a^3}{3r}, & r > a, \end{cases} \qquad (4)$$

where $n = N/\mathcal{V}$ is the electronic density and $\mathcal{V} = 4\pi a^3/3$ the volume of the particle. The potential U is harmonic inside the particle and Coulomb-like outside it.

The experimentally obtained photoabsorption cross section is dominated by the surface plasmon (SP) resonance at the frequency $\omega_{\rm M}$. The width Γ of this resonance can, in principle, be calculated from the eigenstates of H appearing in Eq. (2). However, this procedure is in general exceedingly difficult, and thus various approximation schemes have been proposed.[2,13] Among them, the TDLDA (time-dependent local density approximation) is a numerical approach based on the local density approximation.[5] We will use this numerical scheme as a check of analytical approaches that instructs us on the physical underlying mechanisms to the plasmon decay.

Since we are in the long-wavelength limit where the field couples only to the electronic center of mass, a particularly useful decomposition of the Hamiltonian (3) is

$$H = H_{\rm cm} + H_{\rm rel} + H_{\rm c}.$$

Introducing the canonical coordinates $(\mathbf{R}, \mathbf{P})$, the (harmonic) center-of-mass Hamiltonian is given by

$$H_{\rm cm} = \frac{P^2}{2Nm_{\rm e}} + \frac{1}{2}Nm_{\rm e}\omega_{\rm M}^2 R^2.$$

$H_{\rm rel}$ is the Hamiltonian of the relative coordinates and $H_{\rm c}$ expresses the coupling between the two subsystems. Introducing the standard position, momentum and lowering operators

$$a_Q = \sqrt{\frac{Nm_{\rm e}\omega_{\rm M}}{2\hbar}}Q + \frac{\mathrm{i}}{\sqrt{2Nm_{\rm e}\hbar\omega_{\rm M}}}P_Q,\ Q = X, Y, Z,$$

we can write

$$\hat{H}_{\rm cm} = \hbar\omega_{\rm M}\sum_{Q=X,Y,Z}\left(a_Q^\dagger a_Q + \frac{1}{2}\right).$$

It is difficult to handle $H_{\rm rel}$ and $H_{\rm c}$ in the general case. A notable exception is that of a confining potential which is not given by Eq. (4), but which is harmonic for all r. We are then in the situation for which Kohn's theorem[19] applies. It states that in a purely harmonic confinement potential, and with interactions only depending on the interparticle distance, the center of mass and the relative coordinates decouple (i.e., $H_{\rm c} = 0$). The motion of the center of mass is that of a harmonic oscillator, with the characteristic frequency of the confining potential, independent of the electron-electron interaction. Due to the decoupling, the SP has an infinite lifetime. Kohn's theorem gives us a first insight into the relaxation process of the SP: The Coulomb part of U (for $r > a$) leads to the coupling of the center of mass and the relative coordinates (i.e. $H_{\rm c} \neq 0$), and translates into the decay of the SP.

For the realistic situation $H_{\rm c} \neq 0$, it is useful to describe $H_{\rm rel}$ and $H_{\rm c}$ within the mean-field approximation, where $H_{\rm rel}$ can be expressed as

$$\hat{H}_{\rm MF} = \sum_\alpha \varepsilon_\alpha c_\alpha^\dagger c_\alpha,$$

where ε_α are the eigenenergies for the mean-field potential V and $c_\alpha^\dagger$ (c_α) creates (annihilates) the one-body eigenstate $|\alpha\rangle$. Consequently, the mean-field approximation to $H_{\rm c}$ will be given by the change δV induced in the one-body potential V by a displacement Z of the center of mass. In Appendix A we show how to obtain δV in a self-consistent way from the electronic Coulomb interactions [Eq. (A2)]. In second quantization, we can write

$$\hat{H}_{\rm c} = \sqrt{\frac{\hbar m_{\rm e}\omega_{\rm M}^3}{2N}}\sum_{\alpha\beta} d_{\alpha\beta}(a_Z^\dagger + a_Z)c_\alpha^\dagger c_\beta, \qquad (5)$$

where $d_{\alpha\beta}$ is the matrix element of the classical dipole field between two eigenstates of the unperturbed mean-field problem [Eq. (A3)].

The laser excitation induces an initial electronic state corresponding to a rigid shift (with a magnitude Z) of the unperturbed ground state. Within our separation for the degrees of freedom of the electronic system, such an initial state can be written as a product of the ground state for the relative coordinate system and a coherent state for the center of mass (along the direction of the excitation). Since the amplitude of the perturbation is assumed to be small, the initial coherent state can be approximated by a linear superposition of the ground state $|0_{\rm cm}\rangle$ and the first (harmonic oscillator) excited state $|1_{{\rm cm},Z}\rangle$. The lifetime of such an initial state is that of the SP. It is related to the transition rate Γ of $|1_{{\rm cm},Z}\rangle$ to $|0_{\rm cm}\rangle$ by $T_1 = \hbar/\Gamma$, while the dephasing time is given by $T_2 = 2T_1$. This decay is due to the coupling $\hat{H}_{\rm c}$ and results in the transition of the relative coordinate system from its ground state to excited ones (that within our mean-field assumption we note $|0_{\rm MF}\rangle$ and $|f_{\rm MF}\rangle$, respectively).

Assuming a weak coupling $\hat{H}_{\rm c}$, the SP linewidth can be obtained from the Fermi Golden Rule as

$$\Gamma = 2\pi\sum_{f_{\rm MF}}\left|\langle 0_{\rm cm}, f_{\rm MF}|\hat{H}_{\rm c}|1_{{\rm cm},Z}, 0_{\rm MF}\rangle\right|^2\delta(\hbar\omega_{\rm M} - \varepsilon_{f_{\rm MF}}).$$

According to form (5) of $\hat{H}_{\rm c}$, the final mean-field states $|f_{\rm MF}\rangle$ are particle-hole excitations, and therefore

$$\Gamma = \frac{\pi\hbar\omega_{\rm M}^3 m_{\rm e}}{N}\sum_{ph}|d_{ph}|^2\,\delta(\hbar\omega_{\rm M} - \varepsilon_p + \varepsilon_h), \qquad (6)$$

where $|p\rangle$ and $|h\rangle$ represent, respectively, particle and hole states of the mean-field problem.

Form (6) of the SP linewidth can also be derived from discrete-matrix random phase approximation[13] using the classical field associated with the collective state as the source of particle-hole transitions. The procedure presented above is easy to generalize for the two cases important for our work: a nonhomogeneous dielectric function and the excitation of the second plasmon.

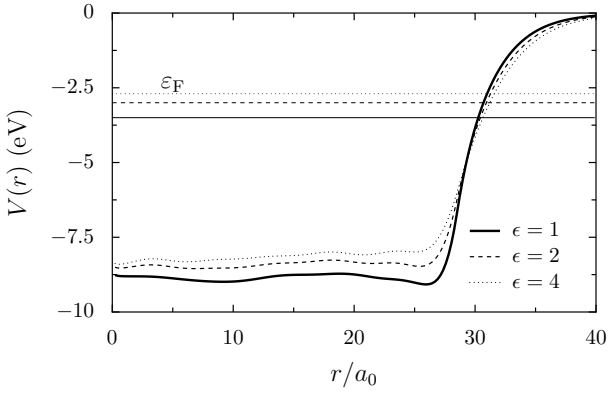

FIG. 1: Self-consistent potential as a function of the radial coordinate (in units of the Bohr radius a_0) from the TDLDA calculations for a 832-atom nanoparticle with mean distance between electrons $r_s = (3/4\pi n)^{1/3} = 3.03\ a_0$, corresponding to $a \simeq 28.5\ a_0$. The different curves are for $\epsilon = \epsilon_d = \epsilon_m$ between 1 and 4, showing that the slope of the potential decreases with increasing values of ϵ. The corresponding Fermi levels are indicated by horizontal lines.

III. SIZE DEPENDENCE OF THE PLASMON LINEWIDTH

In order to evaluate the plasmon linewidth from Eq. (6), we need a description of the eigenstates $|\alpha\rangle$ (p or h) of the mean-field problem. The self-consistent potential obtained from TDLDA (thick line, Fig. 1) suggests that for analytical calculations, $V(r)$ can be approximated by a spherical well of radius a and finite height V_0:

$$V(r) = V_0\Theta(a-r), \tag{7}$$

with Θ the Heaviside distribution. This stair like approximation becomes more appropriate as the particle size increases. As we discuss in the next chapter, the dielectric constants inside and outside the cluster influence the steepness of $V(r)$.

The spherical symmetry of the problem allows us to separate the wave functions and matrix elements into radial and angular components

$$\psi_{klm}(\mathbf{r}) = \frac{u_{kl}(r)}{r} Y_l^m(\Omega),$$

and

$$d_{\alpha\beta} = \mathcal{A}_{l_\alpha l_\beta}^{m_\alpha m_\beta} \mathcal{R}_{k_\alpha k_\beta}^{l_\alpha l_\beta}. \tag{8}$$

u_{kl} satisfies the radial Schrödinger equation (B1), Y_l^m represents the spherical harmonics, $k = (2m_e\varepsilon)^{1/2}/\hbar$ is given by the principal quantum number, while l and m are the angular momentum quantum numbers. The angular part of the matrix element can be expressed in terms of the Wigner-3j symbols as

$$\begin{aligned}\mathcal{A}_{l_\alpha l_\beta}^{m_\alpha m_\beta} =& (-1)^{m_\alpha}\sqrt{(2l_\alpha+1)(2l_\beta+1)} \\ &\times \begin{pmatrix} l_\alpha & l_\beta & 1 \\ 0 & 0 & 0 \end{pmatrix} \begin{pmatrix} l_\alpha & l_\beta & 1 \\ -m_\alpha & m_\beta & 0 \end{pmatrix}.\end{aligned} \tag{9}$$

The dipole matrix element of the radial problem can be written as

$$\mathcal{R}_{k_\alpha k_\beta}^{l_\alpha l_\beta} = \frac{\hbar^2}{m_e(\varepsilon_\alpha - \varepsilon_\beta)^2} \int_0^\infty \mathrm{d}r\ u_{k_\alpha l_\alpha}^*(r)\ \frac{\mathrm{d}V}{\mathrm{d}r}\ u_{k_\beta l_\beta}(r). \tag{10}$$

In the limit of large V_0, we have $u_{kl}(r) = \sqrt{2}[a^{3/2} j_{l+1}(ka)]^{-1} r\, j_l(kr)$, where j_l are the spherical Bessel functions and the allowed values of k are given by the quantization condition $j_l(ka) = 0$, one obtains[13]

$$\mathcal{R}_{k_p k_h}^{l_p l_h} = \frac{2\hbar^2}{m_e a} \frac{\sqrt{\varepsilon_p \varepsilon_h}}{(\varepsilon_p - \varepsilon_h)^2}. \tag{11}$$

The summations appearing in Eq. (6) can be replaced by integrals provided one knows the particle (and hole) density of states (DOS). Decomposing the latter as a sum over its fixed angular momentum components [$\varrho(\varepsilon) = \sum_{l=0}^\infty \sum_{m=-l}^{+l} \varrho_l(\varepsilon)$], we have

$$\begin{aligned}\Gamma = 2\frac{4\pi\hbar}{N m_e a^2 \omega_M} \int_{\max(\varepsilon_F, \hbar\omega_M)}^{\varepsilon_F + \hbar\omega_M} \mathrm{d}\varepsilon_p\ \varepsilon_p \varepsilon_h \\ \times \sum_{\substack{l_p, m_p \\ l_h, m_h}} \varrho_{l_p}(\varepsilon_p)\varrho_{l_h}(\varepsilon_h) \left(\mathcal{A}_{l_p l_h}^{m_p m_h}\right)^2,\end{aligned}$$

with $\varepsilon_h = \varepsilon_p - \hbar\omega_M$. The overall factor of 2 accounts for the spin degeneracy. The angular part (9) of the dipole matrix element contains the selection rules $m_h = m_p$ and $l_h = l_p \pm 1$. Performing the sum over m_p and l_h, with the change of variables $\varepsilon_p = \varepsilon_0 \eta_p^2$, $\varepsilon_h = \varepsilon_0 \eta_h^2$ ($\varepsilon_0 = \hbar^2/2m_e a^2$ and $\eta = ka$), we have

$$\begin{aligned}\Gamma =& 4\varepsilon_0^2 \gamma \int_{\eta_p^{\min}}^{\eta_p^{\max}} \mathrm{d}\eta_p\ \eta_p^3 {\eta_h}^2 \\ &\times \sum_{l_p} \left[l_p \varrho_{l_p-1}(\eta_h) + (l_p+1)\varrho_{l_p+1}(\eta_h)\right] \varrho_{l_p}(\eta_p),\end{aligned} \tag{12}$$

where $\gamma = 2\pi\hbar^3/3N m_e^2 \omega_M a^4$, $\eta_p^{\min} = \eta_F \max(1, \sqrt{\xi})$, $\eta_p^{\max} = \eta_F\sqrt{1+\xi}$, $\xi = \hbar\omega_M/\varepsilon_F$ and $\eta_F = k_F a$.

The SP linewidth depends on the l-fixed DOS of the particles and holes. The asymptotic distributions of the zeros of the Bessel functions were used in Refs. 12 and 13 to obtain the leading behavior of Γ for the largest radii of the considered interval. Corrections, relevant for smaller radii, necessitate numerical or semiclassical approaches.

A. Semiclassical approach and smooth size-dependent component of the plasmon linewidth

The semiclassical approximation to the radial problem (see Appendix B) allows us to write the l-fixed DOS as

$$\varrho_l(\varepsilon) = \frac{\tau_l(\varepsilon)}{2\pi\hbar}\left\{1 + 2\sum_{\tilde{r}=1}^{\infty}\cos\left[\tilde{r}\left(\frac{S_l(\varepsilon)}{\hbar} - \frac{3\pi}{2}\right)\right]\right\}. \quad (13)$$

The classical action of the periodic orbit at energy ε is

$$S_l(\varepsilon) = 2\hbar\Bigg[\sqrt{(ka)^2 - (l+1/2)^2} - \left(l+\frac{1}{2}\right)\arccos\left(\frac{l+1/2}{ka}\right)\Bigg],$$

while its period is given by

$$\tau_l(\varepsilon) = \frac{\hbar\sqrt{(ka)^2 - (l+1/2)^2}}{\varepsilon_0 (ka)^2},$$

and we note $\tilde{r}$ the number of repetitions of the periodic orbit. Within the semiclassical approximation, the finite height V_0 of the self-consistent potential is irrelevant since the classical trajectories at a given energy are not sensitive to the shape of the potential above this energy.

In the semiclassical approach of Ref. 15, that we extend and improve in the sequel, it is natural to decompose the DOS into a smooth part ϱ_l^0 and an oscillating part $\varrho_l^{\rm osc}$ [Eqs. (13) and (B3)]. With Eq. (12), this leads to the dominant (smooth $1/a$-dependent) component of Γ (due to the terms $\varrho_{l_p}^0 \varrho_{l_h}^0$ of the product) with nonmonotonous (in a) corrections.

For the smooth part, we assume that $l_p \gg 1$, consistent with the fact that we are interested in leading order contributions in $\hbar$. Then we use $l_h \pm 1 \simeq l_p$ and approximate the sum over l_p by an integral. Setting $y = l_p^2/\eta_{\rm F}^2$ and $z = \eta_p^2/\eta_{\rm F}^2$, we find

$$\Gamma^0(a) = \frac{\gamma(k_{\rm F}a)^6}{2\pi^2}\int_{\max(1,\xi)}^{1+\xi} {\rm d}z \int_0^{z-\xi} {\rm d}y \sqrt{z-y}\sqrt{z-y-\xi}. \quad (14)$$

Performing the integrals of Eq. (14) leads to the smooth component Γ^0 given by Eq. (1). The $1/a$ dependence agrees with the linear-response result of Kawabata and Kubo.[11] The function g appearing in Eq. (1) decreases with ξ with $g(0) = 1$ and $\lim_{\xi\to\infty} g(\xi) = 0$. Its explicit form can be found in Refs. 12 and 13; it is reproduced in Fig. 5 of Appendix C.

The smooth component of the linewidth of the collective state is inversely proportional to the radius of the nanoparticle: This has been interpreted[11] as a surface effect arising from the confinement of the single-particle states. The analytical evaluation of Γ^0 agrees with the numerical calculations (see dashed line of Fig. 2). Experiments on charged alkaline clusters with a diameter in the range 1–5 nm in vacuum[6] yield a linewidth of the order of $\Gamma \sim 1$ eV. Although the charged character of those clusters limits the applicability of our model, we note that our calculated value is smaller, but of the same order of magnitude than the experimental one. This difference might be explained by additional contributions to the linewidth present in the experiment.

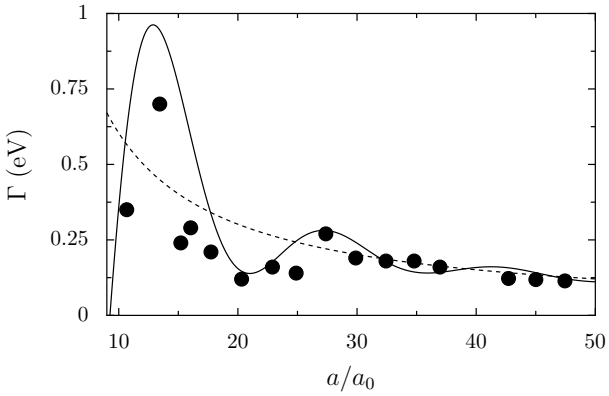

FIG. 2: Inverse lifetime of the first collective excitation in Na nanoparticles as a function of the radius a of the particle. The dashed line is the smooth part of the single plasmon linewidth, Eq. (1). The full line is the smooth part plus the oscillating contribution from Eq. (18) for a number of repetitions $\tilde{r} = 1$. This semiclassical result is compared to numerical TDLDA calculations (dots) for clusters with magic numbers of atoms between 20 and 1760.

B. Shell effects and nonmonotonic behavior of the plasmon linewidth

The oscillating part of the DOS (13) gives rise to terms of the type $\varrho_l^0 \varrho_{l'}^{\rm osc}$ as well as $\varrho_l^{\rm osc}\varrho_{l'}^{\rm osc}$. The former become negligible (in the semiclassical limit of small $\hbar$) in Eq. (12) because one integrates a smooth function multiplied by a highly oscillating one. The latter yield

$$\Gamma^{\rm osc} = \frac{4\gamma}{\pi^2}\int_{\eta_p^{\min}}^{\eta_p^{\max}} {\rm d}\eta_p \eta_p \sum_{\substack{l_p \\ l_h = l_p \pm 1}} f_{l_h} \prod_{\alpha=p,h}\sqrt{\eta_\alpha^2 - (l_\alpha + 1/2)^2} \times \sum_{\tilde{r}_\alpha \geqslant 1}\cos\left[\tilde{r}_\alpha\left(\frac{S_{l_\alpha}(\eta_\alpha)}{\hbar} - \frac{3\pi}{2}\right)\right],$$

where $f_{l_h} = l_p$ for $l_h = l_p - 1$ and $f_{l_h} = l_p + 1$ for $l_h = l_p + 1$. We can expand the product of the two cosines and keep only the contribution in leading order in $\hbar$, neglecting the highly oscillating term as a function of the particle and hole actions. We now write this contribution with the

help of the Poisson summation rule to obtain

$$\Gamma^{\rm osc} \simeq \frac{\gamma}{\pi^2}\int_{\eta_p^{\rm min}}^{\eta_p^{\rm max}} {\rm d}\eta_p\eta_p \sum_{\tilde m=-\infty}^{+\infty}\sum_{\substack{\tilde r_p,\tilde r_h\geqslant 1\\ \sigma=\pm}}\int_{-1/2}^{l_{\rm max}}{\rm d}l_p$$
$$\times \sum_{l_h=l_p\pm 1} f_{l_h}\prod_{\alpha=p,h}\sqrt{\eta_\alpha^2-(l_\alpha+1/2)^2}\,{\rm e}^{\sigma {\rm i}\phi_{l_p}^{\tilde r_p\tilde r_h\tilde m}(\eta_p)}, \quad (15)$$

where we have defined the phase

$$\phi_{l_p}^{\tilde r_p\tilde r_h\tilde m}(\eta_p) = \frac{\tilde r_p S_{l_p}(\eta_p)}{\hbar}-\frac{\tilde r_h S_{l_h}(\eta_h)}{\hbar} - \frac{3\pi}{2}(\tilde r_p-\tilde r_h)+2\pi\tilde m l_p. \quad (16)$$

Performing a stationary phase approximation, given by the condition $\partial\phi/\partial l_p|_{\bar l_p}=0$ with the stationary points $\bar l_p$, we obtain the stationary phase equation

$$\tilde r_p \arccos\left(\frac{\bar l_p+1/2}{\eta_p}\right)-\tilde r_h\arccos\left(\frac{\bar l_h+1/2}{\eta_h}\right)=\pi\tilde m.$$

The phase of Eq. (16) indicates that the major contribution to the integral over l_p in Eq. (15) will be given by $\tilde r_p=\tilde r_h$ and $\tilde m=0$. We then select only one point within the full mesh of the stationary points,

$$\frac{\bar l_p+1/2}{\eta_p}=\frac{\bar l_h+1/2}{\eta_h}. \quad (17)$$

Noticing that $\eta_h=(\eta_p^2-\eta_{\rm F}^2\xi)^{1/2}<\eta_p$, we see that in order to satisfy Eq. (17), we have to set $\bar l_h=\bar l_p-1$. The stationary point is then given by

$$\bar l_p=\frac{\eta_p+\eta_h}{2(\eta_p-\eta_h)}.$$

Performing the integral over l_p with the help of the stationary phase approximation finally provides the following result for the oscillating part of the first plasmon linewidth:

$$\Gamma^{\rm osc}(a) = 6\sqrt{\pi}\frac{\varepsilon_{\rm F}}{\xi(k_{\rm F}a)^5}\int_{\max(1,\sqrt{\xi})}^{\sqrt{1+\xi}}{\rm d}\beta\frac{\beta+\beta'}{(\beta-\beta')^4} \times\beta^{5/2}\beta'^{3/2}\left[(k_{\rm F}a)^2(\beta-\beta')^2-1\right]^{5/4} \times\sum_{\tilde r=1}^{\infty}\frac{1}{\sqrt{\tilde r}}\cos\left\{2\tilde r\Big[\sqrt{(k_{\rm F}a)^2(\beta-\beta')^2-1} -\arccos\left(\frac{1}{k_{\rm F}a(\beta-\beta')}\right)\Big]-\frac{\pi}{4}\right\}, \quad (18)$$

where $\beta'=\sqrt{\beta^2-\xi}$ and $\xi=\hbar\omega_{\rm M}/\varepsilon_{\rm F}$. The remaining integral over β can be performed numerically (solid line, Fig. 2). Assuming that $k_{\rm F}a\gg 1$, using that $\beta-\beta'\sim 1$ and that the sum over the number of repetitions is dominated by the first term, we see that the argument of the cosine is close to $2k_{\rm F}a$ and

$$\Gamma^{\rm osc}(a)\sim\frac{\varepsilon_{\rm F}}{(k_{\rm F}a)^{5/2}}\cos(2k_{\rm F}a).$$

Therefore the linewidth of the single SP excitation has a nonmonotonic behavior as a function of the size a of the metallic cluster. This is due to the density-density particle-hole correlation appearing in the Fermi Golden Rule (6). Let us mention that the result of Eq. (18) is slightly different from the one of our previous work.[15] This is due to the fact that we have used here a more rigorous treatment of the semiclassical radial problem. As in Ref. 15, we have to set a phase shift in our analytical prediction of Eq. (18) to map the TDLDA numerical points in Fig. 2. This is due to the fact that we have taken only one stationary point [Eq. (17)] and neglected all the other contributions coming from the full mesh of stationary points which influence the phase appearing in Eq. (15).

A nonmonotonic behavior has also been observed experimentally in the case of charged lithium clusters.[6] Our numerical TDLDA calculations (that we have extended here to larger sizes, up to 1760 atoms) confirm the presence of size-dependent oscillations for alkaline metals. The semiclassical approach also predicts a nonmonotonous behavior of Γ for noble metal clusters, in agreement with recent experimental results.[20] However, the presence of different dielectric constants inside and outside the cluster render the problem more involved. This issue is discussed in the following section.

IV. PLASMON LINEWIDTH WITH AN INHOMOGENEOUS DIELECTRIC ENVIRONMENT

In a previous analysis of the surface plasmon (SP) linewidth,[15] we were interested by the case of noble metallic nanoparticles (where the d electrons are modeled via a dielectric constant $\epsilon_{\rm d}$) embedded in a matrix of dielectric constant $\epsilon_{\rm m}$. The two dielectric constants affect $\omega_{\rm M}$ as discussed in the introduction. However, a generalization of the derivation of Sec. III shows that, as long as we work with the hypothesis of a steep potential [Eq. (7)], the smooth part of Γ is still given by Eq. (1). For a silver nanoparticle ($\epsilon_{\rm d}\simeq 3.7$) embedded in an argon matrix ($\epsilon_{\rm m}\simeq 1.7$),[21] using Eq. (1) yields a value of Γ^0 about three times larger than the TDLDA calculations[15] (themselves in good agreement with existing experiments[7]). This discrepancy makes the more systematic study of the dependence of the plasmon lifetime on $\epsilon_{\rm d}$ and $\epsilon_{\rm m}$ presented in this section necessary.

In Fig. 3(a) we present the SP linewidth obtained from TDLDA for several particle sizes between $N=138$ and 1760, taking $\epsilon_{\rm d}=4$ and $\epsilon_{\rm m}=2$ and the electron density of silver ($r_{\rm s}=3.03\ a_0$). As in the case of Fig. 2, we see that for relatively large radii the linewidth can be approximated by $\Gamma^0=C/(a/a_0)$ while for smaller radii a, superimposed oscillations become noticeable. As shown in Fig. 3(b), when plotting the coefficients C as a function of $\epsilon_{\rm d}$ and $\epsilon_{\rm m}$, we see that the numerical results are at odds with the simple prediction of Eq. (1) (upward continuous

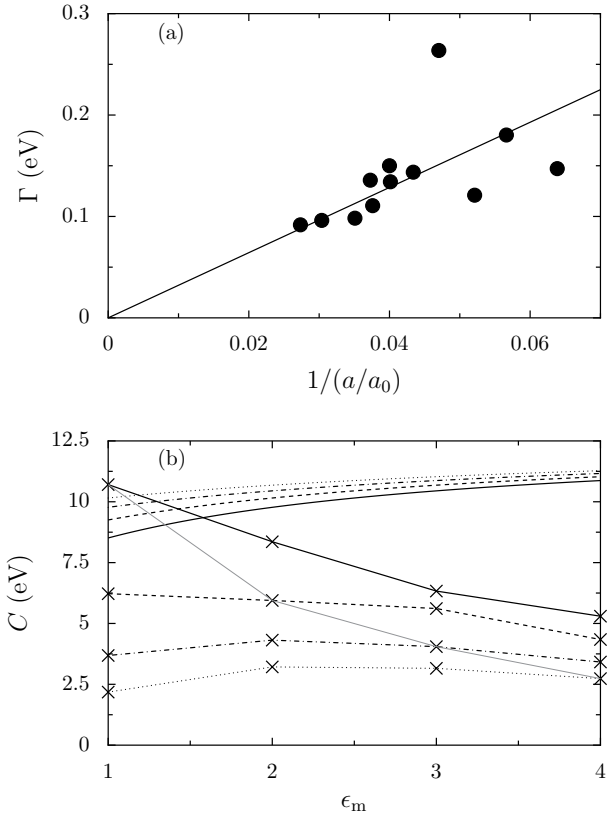

FIG. 3: (a) Surface plasmon linewidth from the TDLDA as a function of the inverse radius for the example of $\epsilon_{\rm d} = 4$ and $\epsilon_{\rm m} = 2$ (dots). The straight line is a linear fit $\Gamma = C/(a/a_0)$. (b) Prefactor C of the smooth $1/a$ size-dependent component of the surface plasmon linewidth Γ^0 as a function of $\epsilon_{\rm m}$ for $\epsilon_{\rm d} = 1$ (solid line), $\epsilon_{\rm d} = 2$ (dashed line), $\epsilon_{\rm d} = 3$ (dashed-dotted line), and $\epsilon_{\rm d} = 4$ (dotted line). The crosses connected by straight lines (guide-to-the-eye) represent the TDLDA calculations, while the increasing curves in the upper part of the figure depict the analytical expression (1). The thin gray line is for $\epsilon_{\rm d} = \epsilon_{\rm m}$. The results presented in the figure are for the electron density of silver ($r_{\rm s} = 3.03\ a_0$).

curves).

The increase of Γ^0 with $\epsilon_{\rm d}$ and $\epsilon_{\rm m}$ in the latter case arises from the fact that the function g is decreasing with $\xi = \hbar\omega_{\rm M}/\varepsilon_{\rm F}$ and the Mie frequency $\omega_{\rm M} = \omega_{\rm p}/\sqrt{\epsilon_{\rm d} + 2\epsilon_{\rm m}}$ is redshifted when $\epsilon_{\rm d}$ or $\epsilon_{\rm m}$ is increasing. Calculations performed for the electronic density of sodium ($r_{\rm s} = 3.93\ a_0$) give the same kind of discrepancy between Eq. (1) and TDLDA results.[22]

The discrepancy between the numerics and Eq. (1) shows that a direct application of the analytical approach presented in the preceeding section does not reproduce the TDLDA results. As we will see in the following, the discrepancy is caused by approximating the electronic self-consistent potential by a square well.

The TDLDA calculations show that the shape of the self-consistent potential is modified when one increases the dielectric constants $\epsilon_{\rm d}$ or $\epsilon_{\rm m}$. In Fig. 1 we present the self-consistent potential of a nanoparticle consisting of $N = 832$ atoms ($r_{\rm s} = 3.03\ a_0$) for various values of $\epsilon = \epsilon_{\rm d} = \epsilon_{\rm m}$. This choice does not correspond to a physical realization, but it is useful for the interpretation of the analytical work, as it merely represents a renormalization of the electronic charge. The main effect of increasing ϵ is the decrease of the slope of the potential near the boundary $r = a$. This indicates that our approximation of a square-well potential becomes less valid as the dielectric constant is increased. The Γ^0 dependence on ϵ in this case is obtained by moving along the line $\epsilon_{\rm d} = \epsilon_{\rm m}$ in Fig. 3(b).

In the following we refine the calculation of the dipole matrix element (10) in order to take into account the behavior of the slope of the self-consistent potential. The finite value of the slope of the self-consistent potential is often ignored. But here, it is necessary to go beyond the hypothesis of infinitely steep potential walls [Eq. (7)] in order to make progress. As it can be seen from Eq. (10), the dipole matrix element is proportional to the matrix element of the derivative of the potential V with respect to r. In the sequel, we show that below a certain value, the dipole matrix element is directly proportional to the slope of the self-consistent potential near the interface and estimate the slope from a simple model. Since the linewidth is proportional to the square of the dipole matrix element, we see that Γ decreases with the slope, and thus with the increase of the dielectric constant.

A. Surface plasmon linewidth with a soft self-consistent potential

In order to improve our understanding of the role of a dielectric mismatch to the SP linewidth, we now need to come back to the evaluation of Eq. (6) without making the approximation of an infinitely steep well for the self-consistent potential. A simplified way of taking into account the noninfinite slope of $V(r)$ is to change Eq. (7) by

$$V(r) = \begin{cases} 0, & 0 \leqslant r < a - \dfrac{d_s}{2}, \\ s\left(r - a - \dfrac{d_s}{2}\right) + V_0, & a - \dfrac{d_s}{2} \leqslant r \leqslant a + \dfrac{d_s}{2}, \\ V_0, & r > a + \dfrac{d_s}{2}, \end{cases}$$

where the distance d_s on which the slope $s = V_0/d_s$ is nonvanishing is assumed to be small as compared to the nanoparticle radius a. We first need an approximation for the dipole matrix element between particle and hole states in that potential. As explained in Appendix B 3, this can be done semiclassically using the limit in which particle and hole states are close in energy [$(\varepsilon_p - \varepsilon_h)/\varepsilon_{\rm F} = \hbar\omega_{\rm M}/\varepsilon_{\rm F} \ll 1$]. This semiclassical approximation relates the dipole matrix element to the Fourier components of the classical trajectory in the one-dimensional effective potential $V_l^{\rm eff}(r)$. As a simplifying

approximation, we neglect the centrifugal part of the effective potential above $r > a - d_s/2$. Integrating the classical equation of motion, we obtain periodic trajectories (for $\varepsilon < V_0$) given by

$$r(t) = \begin{cases} \sqrt{\dfrac{2\varepsilon}{m_\mathrm{e}}t^2 + \dfrac{\hbar^2(l+1/2)^2}{2m_\mathrm{e}\varepsilon}}, & t \leqslant t_\mathrm{c}, \\ -\dfrac{s}{2m_\mathrm{e}}\left(\dfrac{\tau_l}{2} - t\right)^2 + a + \dfrac{d_s}{2} - \dfrac{V_0 - \varepsilon}{s}, & t > t_\mathrm{c}, \end{cases}$$

with $r(t_\mathrm{c}) = a - d_s/2$ and where τ_l is the period. We can now evaluate the dipole matrix element using the semiclassical Eq. (B7), neglecting the acceleration of the particle for $r - a + d_s/2 \to 0^-$ (justified for $a \gg d_s$). An expansion in $1/\Delta n$ (where Δn is the difference between the radial quantum number of the particle and of the hole) gives, up to an irrelevant phase factor

$$\mathcal{R}^{l_p l_h}_{k_p k_h} \simeq \frac{s}{m_\mathrm{e}}\frac{2}{\tau_{l_p}}\frac{\hbar^3}{(\varepsilon_p - \varepsilon_h)^3}\sin\left(\pi\Delta n\frac{\delta t}{t_\mathrm{c}}\right), \tag{19}$$

with $\delta t = \tau_{l_p}/2 - t_\mathrm{c}$ the time spent by the particle in the region where the slope is nonvanishing.

An estimation of the argument of the sine gives $(\hbar\omega_\mathrm{M}/\Delta)(d_s/a)$, with Δ the mean level spacing. Typical values give $\hbar\omega_\mathrm{M}/\Delta \sim 10^4 \gg 1$. In the limit of a very large slope, d_s/a tends to zero. Then, the argument of the sine is very small compared to one, and we recover the semiclassical evaluation of Eq. (B8) with an infinite slope. On the contrary, if we assume that d_s is of the order of the spillout length[23] ($\sim a_0$), the argument of the sine is much greater than one. Inserting Eq. (19) into Eq. (6), we obtain

$$\Gamma^0 = \frac{2s^2}{\pi\hbar\omega_\mathrm{M}^3 N m_\mathrm{e}}\int_{\varepsilon_\mathrm{F}}^{\varepsilon_\mathrm{F}+\hbar\omega_\mathrm{M}} \mathrm{d}\varepsilon_p \sum_{\substack{l_p,m_p \\ l_h,m_h}} \left(\mathcal{A}^{m_p m_h}_{l_p l_h}\right)^2 \sin^2\left(\pi\Delta n\frac{\delta t}{t_\mathrm{c}}\right).$$

Averaging the highly oscillating sine (squared) by 1/2 gives for the SP linewidth in the limit $\xi \to 0$

$$\Gamma^0(a) \simeq \frac{3s^2}{4}\frac{1}{m_\mathrm{e}\omega_\mathrm{M}^2}\frac{1}{k_\mathrm{F}a}. \tag{20}$$

We then see that in the case of a soft self-consistent potential, the SP linewidth is proportional to the square of the slope s of that potential. When one increases the dielectric constant of the medium, the slope decreases (see Fig. 1) and therefore Γ^0 decreases. We also notice that the smooth $1/a$ size dependence of the SP linewidth remains valid even for a finite slope.

B. Steepness of the self-consistent potential with a dielectric mismatch

In order to estimate the slope of the self-consistent potential, we consider the simpler geometry of a metallic slab of dielectric constant ϵ_d, bounded by two interfaces at $x = \pm w/2$ and with an infinite extension in the (y, z) plane, surrounded by a dielectric medium with a constant ϵ_m. This geometry allows us to simplify the problem to an effective one-dimensional system and can be expected to provide a good approximation for the shape of the potential near the interface for the sphere geometry.

We make the jellium approximation for the ionic density $n_\mathrm{i}(x) = n_\mathrm{i}\Theta(w/2 - |x|)$, with Θ the step function, and work within the Thomas-Fermi approach, writing the local energy in the electrostatic field ϕ as

$$\varepsilon = \frac{p^2(x)}{2m_\mathrm{e}} - e\phi(x),$$

and the electronic density (at zero temperature) as

$$n_\mathrm{e}(x) = \frac{1}{3\pi^2}\left(\frac{2m_\mathrm{e}}{\hbar^2}\right)^{3/2}\left[\mu + e\phi(x)\right]^{3/2},$$

with μ the chemical potential in the potential $V(x) = -e\phi(x)$. The Thomas-Fermi approach to surfaces is known to have serious shortcomings[24] (for instance, it predicts a vanishing work function). However, it will be useful for our estimation of the slope of the mean field seen by the charge carriers. The self-consistency is achieved through the Poisson equation

$$\frac{\mathrm{d}^2\phi}{\mathrm{d}x^2} = \begin{cases} \dfrac{4\pi e}{\epsilon_\mathrm{d}}\left[n_\mathrm{e}(x) - n_\mathrm{i}\right], & |x| < \dfrac{w}{2}, \\ \dfrac{4\pi e}{\epsilon_\mathrm{m}}n_\mathrm{e}(x), & |x| > \dfrac{w}{2}. \end{cases} \tag{21}$$

First we consider the simpler case where $\epsilon_\mathrm{d} = \epsilon_\mathrm{m} = \epsilon$. In this case, integrating once Eq. (21) and invoking the continuity of the potential and the electrical field, we find for the slope of the self-consistent field at $x = w/2$

$$s = \frac{4e}{\sqrt{15\pi}}\left(\frac{2m_\mathrm{e}}{\hbar^2}\right)^{3/4}\frac{\mu_1^{5/4}}{\epsilon^{7/4}}\left[1 - \frac{2}{5\epsilon^{3/2}}\left(\frac{\mu_1}{\varepsilon_\mathrm{F}}\right)^{3/2}\right]^{5/4}, \tag{22}$$

where we have assumed the scaling $\mu \approx \mu_1/\epsilon$ with μ_1 the chemical potential in the case where $\epsilon = 1$, and ε_F is the Fermi energy of the free electron gas. The chemical potential is fixed by the consistency condition

$$\sqrt{\frac{\epsilon\mu}{8\pi e^2 n_\mathrm{i}}}\int_{1-\frac{2}{5}\left(\frac{\mu}{\varepsilon_\mathrm{F}}\right)^{3/2}}^{1}\frac{\mathrm{d}u}{f(u)} = \frac{w}{2} \tag{23}$$

with

$$f(u) = \sqrt{\frac{2}{5}\left(\frac{\mu}{\varepsilon_\mathrm{F}}\right)^{3/2}(u^{5/2} - 1) - (u - 1)}.$$

If we do not have any dielectric constant (i.e., $\epsilon = 1$), the same equation is obtained but without the prefactor $\sqrt{\epsilon}$. The integral in Eq. (23) is clearly dominated by its prefactor. Then, assuming that the integral appearing

in this equation does not change appreciably when we have a dielectric constant, we find the scaling $\mu \approx \mu_1/\epsilon$. Therefore, we see that the slope at the interface is decreasing with increasing values of the dielectric constant ϵ, a feature confirmed by our TDLDA calculations (see Fig. 1).

In the case where we have a dielectric mismatch between the metallic slab and the environment, the continuity of the normal component of the displacement field $\mathbf{D}$ gives, perturbatively, in the limit $|\epsilon_\mathrm{d} - \epsilon_\mathrm{m}| \to 0$,

$$s = \frac{4e}{\sqrt{15\pi}} \left(\frac{2m_\mathrm{e}}{\hbar^2}\right)^{3/4} \frac{\mu_1^{5/4}}{\epsilon_\mathrm{m}^{1/2}\epsilon_\mathrm{d}^{5/4}} \left[1 - \frac{2}{5\epsilon_\mathrm{d}^{3/2}} \left(\frac{\mu_1}{\varepsilon_\mathrm{F}}\right)^{3/2}\right]^{5/4} \times \left\{1 + \frac{\epsilon_\mathrm{d} - \epsilon_\mathrm{m}}{2\epsilon_\mathrm{d}^{5/2}} \left(\frac{\mu_1}{\varepsilon_\mathrm{F}}\right)^{3/2} \left[1 - \frac{2}{5\epsilon_\mathrm{d}^{3/2}} \left(\frac{\mu_1}{\varepsilon_\mathrm{F}}\right)^{3/2}\right]\right\}, \tag{24}$$

with the scaling $\mu \approx \mu_1/\epsilon_\mathrm{d}$, which can be justified in the same manner as for the case of a single dielectric constant. The only difference is that in the case of a dielectric mismatch, we obtain Eq. (23), up to a change of ϵ by ϵ_d. We then see that the slope s of the confining mean-field potential at the interface is decreasing either with ϵ_d or ϵ_m (for small $|\epsilon_\mathrm{d} - \epsilon_\mathrm{m}|$), in agreement with the TDLDA calculations.

This Thomas-Fermi approach to the mean-field potential of a metallic slab then provides an estimate of the slope of that potential near the interface between the slab and the surrounding environment. It can be expected that these results are also applicable to the more involved problem of the metallic sphere, up to some geometrical prefactors. In the following section, we will incorporate our estimate of the self-consistent potential slope in our evaluation of the SP lifetime.

C. Surface plasmon linewidth with a dielectric mismatch

We can now use our estimate (24) for the slope of the self-consistent potential in our evaluation (20) of the SP linewidth. In order to do that, we assume that the chemical potential μ_1 for $\epsilon = 1$ is the Fermi energy ε_F of a free electron gas.

In the case where we have a charge renormalization (i.e., $\epsilon_\mathrm{d} = \epsilon_\mathrm{m} = \epsilon$), we obtain by inserting Eq. (22) into Eq. (20)

$$\Gamma^0(a) \simeq \frac{9}{5} \frac{\varepsilon_\mathrm{F}}{k_\mathrm{F} a} \frac{1}{\epsilon^{5/2}} \left(1 - \frac{2}{5\epsilon^{3/2}}\right)^{5/2}. \tag{25}$$

This result qualitatively reproduces the decrease obtained from TDLDA for $\Gamma^0\, a/a_0$ as a function of the dielectric constant ϵ as it can be seen on Fig. 3(b) (gray thin line). We notice that for $\epsilon = 1$, we have $\Gamma^0 \approx \varepsilon_\mathrm{F}/k_\mathrm{F} a$ in the limit of small ξ, which has to be compared with Eq. (1) giving $1.5\ \varepsilon_\mathrm{F}/k_\mathrm{F} a$. This small discrepancy is not surprising, regarding the various approximations we made here.

In the case where we have a dielectric mismatch, by inserting Eq. (24) into Eq. (20) and making the expansion for small $\Delta\epsilon = \epsilon_\mathrm{d} - \epsilon_\mathrm{m}$, we obtain

$$\Gamma^0(a) \simeq \Gamma^0_{(\Delta\epsilon=0)}(a) + A\Delta\epsilon \tag{26}$$

for fixed ϵ_d and

$$\Gamma^0(a) \simeq \Gamma^0_{(\Delta\epsilon=0)}(a) - B\Delta\epsilon \tag{27}$$

for fixed ϵ_m. In the above two equations, A and B are two positive coefficients not specified here, and $\Gamma^0_{(\Delta\epsilon=0)}$ is given by Eq. (25). These results confirm the behavior of the TDLDA calculations depicted on Fig. 3(b) around $\Delta\epsilon = 0$ (thin gray line). For instance, if we are at ϵ_m fixed, we see that when $\Delta\epsilon > 0$, Eq. (27) predicts that $\Gamma^0\, a/a_0$ decreases for increasing value of ϵ_d.

We have shown in this section how to take into account an inhomogeneous dielectric environment in our semiclassical model through the corrections in the slope of the mean-field potential. This improved theory is in qualitative agreement with the TDLDA calculations.

V. HIGHER COLLECTIVE EXCITATIONS: DOUBLE PLASMON

In this section we discuss the lifetime of the second collective excitation level in metallic nanoparticles. Although there is no clear direct experimental observation of a double plasmon in metallic clusters, the development of femtosecond spectroscopy will certainly allow for detailed studies in the near future. Recent experiments observed the ionization of the charged cluster Na_{93}^+ by a femtosecond laser pulse and claimed it was a consequence of the excitation of the second plasmon state.[17a] However, the analysis of the distribution of photoelectrons yielded a thermal distribution and therefore the relevance of the double plasmon for this experiment is not yet settled.[17b] On the other hand, it is clear that a strong-enough laser pulse will excite the second collective state. Such an excitation will be a well-defined resonance only if its linewidth is small compared with other scales of the photoabsorption spectrum (like for instance ω_M).

Second collective excitations have been widely analyzed in the context of giant dipolar resonances in nuclei.[25] The anharmonicities were found to be relatively small, making it possible to observe this resonance.[26] The theoretical tools developed in nuclear physics have been adapted to the study of the double plasmon in metallic clusters.[27,28] In particular, a variational approach[28] showed that the difference between the energy of the double plasmon and $2\hbar\omega_\mathrm{M}$ decreases as $N^{-4/3}$ with the size of the nanoparticle. In our calculations, we will assume that the double-plasmon energy is exactly twice the Mie energy.

For most of the clusters of experimental interest, $2\hbar\omega_{\rm M} > W > \hbar\omega_{\rm M}$, where W is the work function. Ionization then appears as an additional decay channel of the double plasmon that competes with the Landau damping, while it is not possible if only the single plasmon is excited.[29]

A. Second plasmon decay: Landau damping

In this section, we consider processes which do not lead to ionization, that is, the final particle energies verify $\varepsilon_p < V_0 = \varepsilon_{\rm F} + W$. A sufficiently strong laser excitation gives rise to an initial center-of-mass state which is a linear superposition of the ground-state $|0_{\rm cm}\rangle$, the first ($|1_{{\rm cm},Z}\rangle$), and the second ($|2_{{\rm cm},Z}\rangle$) harmonic oscillator excited states.

The second plasmon state can decay by two distinct Landau damping processes. A first-order process, with a rate $\Gamma_{2\to1}$, results from the transition of $|2_{{\rm cm},Z}\rangle$ (double plasmon) into $|1_{{\rm cm},Z}\rangle$ (single plasmon). The corresponding matrix element of the perturbation $\hat{H}_{\rm c}$ between these two states is a factor of $\sqrt{2}$ larger than the one worked in Sec. II, and then $\Gamma_{2\to1} = 2\Gamma$ [where Γ is the single-plasmon linewidth given by Eq. (6) and calculated under certain approximations in Sec. III]. Thus, the contribution of the first-order process to the linewidth is just twice that of the single plasmon, and shows the same nonmonotonic features superposed to a $1/a$ size-dependence.

The other mechanism one has to take into account is the second-order process, where the double plasmon decays directly into the center-of-mass ground state. This is possible provided that $V_0 > 2\hbar\omega_{\rm M}$. In order to simplify the calculation we assume, for the remaining of this section, that $V_0 \to \infty$. The corresponding linewidth $\Gamma_{2\to0}$ is given by the Fermi Golden Rule in second order in perturbation theory by[16]

$$\Gamma_{2\to0} = 2\pi \sum_{f_{\rm MF}} \left| \sum_{f'_{\rm MF}} \frac{\langle 0_{\rm cm}, f_{\rm MF}|\hat{H}_{\rm c}|1_{{\rm cm},Z}, f'_{\rm MF}\rangle\langle 1_{{\rm cm},Z}, f'_{\rm MF}|\hat{H}_{\rm c}|2_{{\rm cm},Z}, 0_{\rm MF}\rangle}{\hbar\omega_{\rm M} - \varepsilon_{f'_{\rm MF}}} \right|^2 \delta(2\hbar\omega_{\rm M} - \varepsilon_{f_{\rm MF}}).$$

Expliciting the perturbation (5) and restricting ourselves to the random phase approximation which allows only one particle-one hole transitions, we obtain

$$\Gamma_{2\to0} = \frac{\pi\hbar^2\omega_{\rm M}^6 m_{\rm e}^2}{N^2} \sum_{ph} |K_{ph}|^2 \, \delta(2\hbar\omega_{\rm M} - \varepsilon_p + \varepsilon_h), \quad (28)$$

with

$$K_{ph} = \sum_{i\neq p,h} \frac{d_{pi} d_{ih}}{\hbar\omega_{\rm M} - \varepsilon_i + \varepsilon_h}. \quad (29)$$

The sum over i runs over all the virtual intermediate states. We use the same notations as in Sec. III and replace the sums over particle and hole states by integrals over the energy with the appropriate density of states (DOS), which is approximated by its semiclassical counterpart.

As in the case of the single plasmon, we work in the limit $l_p \gg 1$ in order to find the smooth size-dependent contribution $\Gamma^0_{2\to0}$ (and the corresponding K^0_{ph}). Using Eqs. (8), (9), (11), and the selection rules, we have

$$K^0_{ph} = \frac{8\hbar^2}{\pi m_{\rm e}\varepsilon_0^2} \Big[\mathcal{A}^{m_p m_p}_{l_p l_p+1} \mathcal{A}^{m_p m_h}_{l_p+1 l_h} I_{l_p+1}(\eta_p,\eta_h)(\delta_{l_h l_p} + \delta_{l_h, l_p+2}) + \mathcal{A}^{m_p m_p}_{l_p l_p-1} \mathcal{A}^{m_p m_h}_{l_p-1 l_h} I_{l_p-1}(\eta_p,\eta_h)(\delta_{l_h l_p} + \delta_{l_h, l_p-2}) \Big] \delta_{m_p m_h}. \quad (30)$$

Here, we have defined the integral

$$I_{l_i}(\eta_p,\eta_h) = \int_{l_i+1/2}^{\infty} {\rm d}\eta_i \frac{\eta_i\sqrt{\eta_i^2 - (l_i+1/2)^2}}{(\xi\eta_{\rm F}^2 - \eta_i^2 + \eta_h^2)\left[(\eta_i^2-\eta_p^2)(\eta_i^2-{\eta_h}^2)\right]^2}.$$

Inserting Eq. (30) into Eq. (28), replacing the sum over l_p by an integral, we find

$$\Gamma^0_{2\to0} = 2\varsigma \int_{\eta_{\rm F}\max(1,\sqrt{2\xi})}^{\eta_{\rm F}\sqrt{1+2\xi}} {\rm d}\eta_p \, \eta_p \times \int_0^{\eta_h} {\rm d}l_p \, l_p \sqrt{\eta_p^2 - l_p^2}\sqrt{{\eta_h}^2 - l_p^2} \left[I_{l_p}(\eta_p,\eta_h)\right]^2,$$

where the factor of 2 accounts for the spin degeneracy. We have introduced $\varsigma = 64(\hbar\omega_{\rm M})^6/5\pi^3 N^2\varepsilon_0^5$ and $\eta_h = (\eta_p^2 - 2\eta_{\rm F}^2\xi)^{1/2}$. With the change of variables $z = \eta_p^2/\eta_{\rm F}^2$, $y = l_p^2/\eta_{\rm F}^2$, and $x = \eta_i^2/\eta_{\rm F}^2$, we obtain

$$\Gamma^0_{2\to0}(a) \simeq \frac{81}{10\pi^3} \frac{\varepsilon_{\rm F}}{(k_{\rm F}a)^2} h(\xi), \quad (31)$$

where the function $h(\xi)$ of the parameter $\xi = \hbar\omega_{\rm M}/\varepsilon_{\rm F}$ is smoothly increasing with $h(0) = 0$. An approximate expression of h is given in Appendix C.

The total linewidth of the Landau damped second plasmon is the sum of the first- and second-order processes: $\Gamma_{\rm DP} = \Gamma_{2\to1} + \Gamma_{2\to0}$. The different (smooth) size dependence of both processes [$v_{\rm F}/a$ for the former and

$(k_{\rm F}a)^{-1}v_{\rm F}/a$ for the latter] implies that, except for the smallest clusters, the second-order process gives a negligible contribution to the linewidth of the double plasmon (in comparison with that of the first order). We might ask the question of whether the inclusion of the oscillating components of both linewidths can affect the above conclusion in this range of particle sizes. An extension of the calculations presented in Sec. III B shows[30] that the oscillating part of the second-order channel of the double plasmon is given by

$$\Gamma^{\rm osc}_{2\to 0}(a) \sim \frac{\varepsilon_{\rm F}}{(k_{\rm F}a)^{11/2}} \cos{(2k_{\rm F}a)}.$$

As indicated before, $\Gamma^{\rm osc}_{2\to 1}$ is given by twice the result of Eq. (18), therefore these nonmonotonic contributions cannot lead to a significant modification of our conclusion about the irrelevance of the second-order term for the sizes of physical interest. We also notice that $\Gamma_{\rm DP} \ll \hbar\omega_{\rm M}$, since for typical nanoparticles, $\varepsilon_{\rm F} \sim \hbar\omega_{\rm M}$ and $k_{\rm F}a \gg 1$. Therefore, the Landau damping is not capable of ruling out the second plasmon as a well-defined resonance.

The lifetime of the second plasmon for the Landau damping processes is simply $\hbar\Gamma^{-1}_{\rm DP}$. From the experimental point of view, what is usually more relevant is the time it takes for the double excited state of the center-of-mass system to return to its ground state rather than the lifetime of the excited state. Therefore, we also have to take into account the decay of the first plasmon into the ground-state $\Gamma_{1\to 0}$. If we assume that the recombination of particle-hole pairs (created by the decay of the double plasmon into the single plasmon) is very fast as compared to other time scales, we have $\Gamma_{1\to 0} = \Gamma$. Due to the fact that lifetimes are additive, we have for this sequential decay a lifetime $\tau_{2\to 1\to 0} = 1.5\hbar\Gamma^{-1}$.

B. Second plasmon decay and ionization

We now examine the last decay channel of the second plasmon state: the relaxation of this collective excitation by ejecting an electron from the nanoparticle (ionization, see inset of Fig. 4). We now need to determine the particle and hole states in the self-consistent field [Eq. (7)] which has a finite height V_0, since the ionization process requires the states of the continuum. For simplicity, we will neglect the Coulomb tail seen for $r > a$ by electrons with an energy $\varepsilon_p > V_0$.

In order to determine the particle and hole states, we close the system into a spherical box of radius $L \gg a$ to quantize the states above the well and take the limit of $L \to \infty$ at the end of our calculations. We need to do some approximations in order to simplify this difficult problem. First, in the high energy limit, we assume that $kr \gg 1$, and then use the asymptotic expansions of the quantum mechanical single-particle states inside and outside the well. Even though this approximation strongly affects the wave functions near $r = 0$, its impact

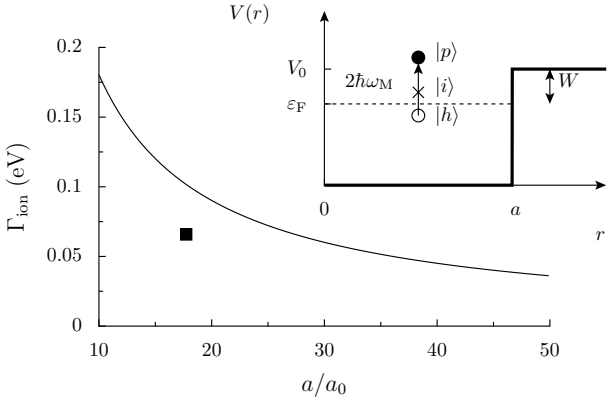

FIG. 4: Ionization linewidth of the second plasmon state as a function of the nanoparticle radius for singly charged Na clusters. Square: experimental value for Na^+_{93} taken from Ref. 17. We have assumed a constant work function $W = 4.65$ eV and took the experimental Mie frequency of 2.75 eV. Inset: scheme of the ionization process of the double-plasmon state which decays by creating a particle-hole pair of energy $2\hbar\omega_{\rm M}$, via the intermediate state $|i\rangle$. Since the energy of the particle is such that $\varepsilon_p > V_0$, ionization occurs.

on the dipole matrix elements is very small.[31] Second, for the states with energy $\varepsilon < V_0$, we neglect the exponential decay of the wave function for $r > a$. Finally, in the spirit of the scattering theory, we use a simplifed expression for the normalization of the free states above the well. The above assumptions result in the following radial wave functions inside the well ($\varepsilon < V_0$)

$$u^{<}_{kl}(r) \simeq \begin{cases} \sqrt{\dfrac{2}{a}} \sin{(kr - l\pi/2)}, & r \leqslant a, \\ 0, & r > a. \end{cases}$$

The wave-vector $k = (2m_{\rm e}\varepsilon)^{1/2}/\hbar$ is given by the quantization condition $ka = l\pi/2 + n\pi$, with n a non-negative integer. Outside of the well ($\varepsilon > V_0$), we have

$$u^{>}_{kl}(r) \simeq \sqrt{\frac{2}{L}} \begin{cases} \alpha_l(k) A(k) \sin{(kr - l\pi/2)}, & r \leqslant a, \\ \sin{[\kappa(r - L)]}, & r > a, \end{cases}$$

with $\kappa = (k^2 - 2m_{\rm e}V_0/\hbar^2)^{1/2}$. We have introduced the abbreviations

$$\alpha_l(k) = \text{sign}\left\{ \frac{\sin{[\kappa(a - L)]}}{\sin{(ka - l\pi/2)}} \right\},$$

$$A(k) = \sqrt{\sin^2{[\kappa(a - L)]} + \left(\frac{\kappa}{k}\right)^2 \cos^2{[\kappa(a - L)]}}.$$

The ionization rate of the double-plasmon state $\Gamma_{\rm ion}$ is given by Eq. (28) in the case where the final particle states p of the sum are in the continuum. Since the effective (second-order) matrix element K_{ph} [Eq. (29)] is given by a sum over intermediate states i, we now have contributions from cases where i lies in the well as well as in the continuum.

When i represents a state in the well, using the angular momentum selection rules, we can write in the limit $kr \gg 1$

$$\mathcal{R}^{l_i l_h}_{k_i k_h} = \frac{(-1)^{n_i - n_h}}{\Delta k_{ih}^2 a} \delta_{l_i, l_h \pm 1}, \tag{32}$$

and

$$\mathcal{R}^{l_p l_i}_{k_p k_i} = \pm \sqrt{\frac{a}{L}} \frac{\alpha_{l_p}(k_p) A(k_p)}{\Delta k_{pi}} \times \left[\cos(\Delta k_{pi} a) - \frac{\sin(\Delta k_{pi} a)}{\Delta k_{pi} a} \right] \delta_{l_i, l_p \pm 1}, \tag{33}$$

where $\Delta k_{\alpha\beta} = k_\alpha - k_\beta$ $(\alpha, \beta = p, h, i)$.

When i represents a state in the continuum, $\mathcal{R}^{l_i l_h}_{k_i k_h}$ can be obtained by exchanging $(p \leftrightarrow i)$ and $(i \leftrightarrow h)$ in Eq. (33). For the remaining case, we have

$$\mathcal{R}^{l_p l_i}_{k_p k_i} \simeq \frac{a}{L} \frac{\alpha_{l_p}(k_p) \alpha_{l_p+1}(k_i) A(k_p) A(k_i)}{\Delta k_{pi}} \times \left[\cos(\Delta k_{pi} a) - \frac{\sin(\Delta k_{pi} a)}{\Delta k_{pi} a} \right] \delta_{l_i, l_p \pm 1} + B(k_p, k_i), \tag{34}$$

where

$$B(k_p, k_i) = \frac{a^2}{L} \Big\{ \cos(\Delta\kappa_{pi} L) - \sin(\Delta\kappa_{pi} L) \mathrm{ci}(|\Delta\kappa_{pi}| a) + \Delta\kappa_{pi} a \big[\cos(\Delta\kappa_{pi} L) \mathrm{sign}(\Delta\kappa_{pi}) \mathrm{si}(|\Delta\kappa_{pi}| a) \big] \Big\},$$

with si and ci the sine and cosine integral functions.

The semiclassical l-fixed smooth DOS can be approximated by

$$\varrho_l^0(\varepsilon) \simeq \frac{1}{2\pi\varepsilon_0} \begin{cases} \dfrac{\sqrt{(ka)^2 - (l+1/2)^2}}{(ka)^2}, & \varepsilon < V_0, \\ \dfrac{\sqrt{(\kappa L)^2 - (l+1/2)^2}}{(\kappa a)^2}, & \varepsilon > V_0. \end{cases}$$

There is an obvious divergency that occurs in the sum of Eq. (29) for $\varepsilon_i = \varepsilon_h$, as it can be seen on the matrix element (32). However, a careful analysis shows that the contribution around that divergency vanishes because of the alternating sign when one integrates over n_i. For $\varepsilon_i = \varepsilon_p$, there is no divergency in Eq. (34). Therefore the dominant contribution to K_{ph} is given by the divergency of the term $1/(\hbar\omega_\mathrm{M} - \varepsilon_i + \varepsilon_h)$ that occurs for $\varepsilon_i < V_0$ in the regime we are interested in $(\hbar\omega_\mathrm{M} < W < 2\hbar\omega_\mathrm{M})$. We then have for the ionization rate

$$\Gamma_\mathrm{ion} \simeq 2 \frac{\pi\hbar^2 \omega_\mathrm{M}^6 m_\mathrm{e}^2}{N^2} \sum_{\substack{p > V_0 \\ h < \varepsilon_\mathrm{F}}} \delta(2\hbar\omega_\mathrm{M} - \varepsilon_p + \varepsilon_h) \times \sum_{i,j < V_0} \frac{d_{pi} d_{ih}}{\hbar\omega_\mathrm{M} - \varepsilon_i + \varepsilon_h} \frac{d_{pj} d_{jh}}{\hbar\omega_\mathrm{M} - \varepsilon_j + \varepsilon_h},$$

where the factor of 2 accounts for the two spin channels and the $d_{\alpha\beta}$ are given by Eq. (8) with the approximations (32) and (33) for the radial matrix elements. Furthermore, we can distinguish in the above equation two contributions: off-diagonal terms $(i \neq j)$ which have divergencies of the principal value type and that we neglect here, and diagonal terms $(i = j)$ yielding divergencies which determine Γ_ion. We smooth out the energy ε_i appearing in the denominator by introducing an imaginary part of the order of the mean level-spacing

$$\Delta = \frac{3\pi\varepsilon_0^{3/2}}{\sqrt{\hbar\omega_\mathrm{M} + \varepsilon_h}}$$

at an energy $\hbar\omega_\mathrm{M} + \varepsilon_h$. This standard procedure of smoothing the divergencies is of critical importance, and that is why in Ref. 16 the final result is presented as a function of Δ. Summing over l_i and m_i, the remaining sum over the radial quantum numbers n_i can be done with the help of

$$\sum_{n_i} \frac{1}{|\hbar\omega_\mathrm{M} - \varepsilon_i + \varepsilon_h + \mathrm{i}\Delta|^2} \approx \frac{\pi}{4\Delta} \frac{1}{\hbar\omega_\mathrm{M} + \varepsilon_h}.$$

For the smooth terms of the sum, we have taken their values at the divergency to obtain

$$\Gamma_\mathrm{ion} \simeq \frac{\pi^2 a (\hbar\omega_\mathrm{M})^6 \varepsilon_0}{120 N^2 L} \sum_{l_p} l_p \int_{\max(V_0, 2\hbar\omega_\mathrm{M})}^{\varepsilon_\mathrm{F} + 2\hbar\omega_\mathrm{M}} \mathrm{d}\varepsilon_p \frac{\varrho_{l_p}(\varepsilon_p) \varrho_{l_p}(\varepsilon_h)}{\Delta} \times \frac{[A(k_p)]^2}{(\hbar\omega_\mathrm{M} + \varepsilon_h)(\sqrt{\hbar\omega_\mathrm{M} + \varepsilon_h} - \sqrt{\varepsilon_h})^4 (\sqrt{\varepsilon_p} - \sqrt{\hbar\omega_\mathrm{M} + \varepsilon_h})^2},$$

with $\varepsilon_h = \varepsilon_p - 2\hbar\omega_\mathrm{M}$.

Taking the limit of $L \to \infty$, we finally obtain

$$\Gamma_\mathrm{ion}(a) \simeq \frac{3\pi}{80} \frac{\varepsilon_\mathrm{F}}{k_\mathrm{F} a} q(\xi, \zeta), \tag{35}$$

where $\xi = \hbar\omega_\mathrm{M}/\varepsilon_\mathrm{F}$ and $\zeta = W/\varepsilon_\mathrm{F}$. The function q of the two variables ξ and ζ is defined in Appendix C, Eq. (C1).

The size scaling of Γ_ion is mainly given by a $1/a$-dependence of the prefactor (Fig. 4), despite the fact that the work function W appearing in the parameter ζ is size dependent and scales (for a neutral cluster) as[32] $W = W_\infty + 3e^2/8a$ where W_∞ is the work function of the bulk material.

Using the work function $W = 4.65$ eV and the experimental value of $\hbar\omega_\mathrm{M} = 2.75$ eV for the charged Na_{93}^+ clusters of Ref. 17, Eq. (35) yields $\Gamma_\mathrm{ion} \simeq 0.1$ eV, which corresponds to an ionization lifetime of the second plasmon of 6.6 fs. This value is of the same order of magnitude as the experimentally reported lifetime of 10 fs. It is also in rough agreement with the estimation yielded by the numerical calculations of Ref. 16 based on a separable residual interaction (10 to 20 fs). Therefore, despite the approximations we have been forced to make in our analytical calculations, we believe that we kept the essential ingredients of this complicated problem. The lifetimes obtained by the different procedures consistently

establish the second plasmon as a well-defined resonance in metallic clusters. While the numerical calculations of Ref. 16 have been performed for just one size, our results exhibit a clear size dependence that can be tested in future experiments.

VI. CONCLUSION

In this work we have analyzed the lifetime of collective excitations in metallic clusters. Different decay mechanisms have been studied within a semiclassical approach for the mean-field self-consistent potential describing the electrons in a jellium background. We have considered Landau damping, which is the dominant relaxation mechanism for nanoparticles with radius a in the range 0.5–2.5 nm. We found that the linewidth of the single surface plasmon exhibits a $1/a$ dependence, superimposed to an oscillating behavior arising from electron-hole density-density correlations. These results are in good agreement with numerical time-dependent local density approximation calculations, and consistent with experiments on free alkaline nanoparticles.

To describe noble metal clusters, we have taken into account the screening effect of the d electrons and the modifications induced by the dielectric properties of an eventual matrix. We have demonstrated that such an inhomogeneous dielectric environment of the nanoparticles strongly affects the steepness of the self-consistent potential, which in turn has a crucial influence on the plasmon linewidth. We could then solve the discrepancy presented in Ref. 15 between the well-known Kawabata and Kubo formula on one side, against experiments and numerical calculations on the other side. The size-dependent oscillations of the linewidth also depend on the dielectric constants through the slope of the self-consistent potential. The access to individual nano-objects, recently developped by different experimental techniques, provides a promising way of testing our theoretical results concerning the size-dependent linewidth oscillations.

The physical relevance of the second plasmon has been analyzed in terms of different decay channels: Landau damping and particle ionization. We have shown that both processes are relevant, but they do not preclude the existence of the resonance. The comparison of our semiclassical calculation with the existing numerical and experimental results is reasonably good, despite the various approximations of our model.

Our theoretical results concerning the different decay mechanisms of the collective excitations of metallic clusters should be important for the analysis of the electron dynamics following short and strong laser excitations.

Acknowledgments

We are grateful to G.-L. Ingold for his careful reading of the manuscript and for illuminating suggestions. We thank G. F. Bertsch, J.-Y. Bigot, and P.-A. Hervieux for useful discussions. We acknowledge the Centre de Coopération Universitaire Franco-Bavarois/Bayerisch-Französisches Hochschulzentrum (CCUFB/BFHZ), the French-German PAI PROCOPE, and the EU (RTN program) for financial support.

APPENDIX A: TRANSITION POTENTIAL

In this Appendix we present the derivation of the transition potential induced by the plasmon field and generalize the derivation of Ref. 3 considering the Coulomb interaction in the case of a dielectric mismatch between the electrons and the surrounding matrix in which the nanoparticles are embedded. Assuming that at equilibrium the electron density is uniform within a sphere of radius a, $n(\mathbf{r}) = n\Theta(a-r)$ (Θ being the Heaviside distribution), a rigid displacement with a magnitude Z along the $\mathbf{e}_z$ direction changes the density at $\mathbf{r}$ from $n(\mathbf{r})$ to

$$n(\mathbf{r}-\mathbf{u}) = n(\mathbf{r}) + \delta n(\mathbf{r}).$$

To first order in the field $\mathbf{u} = Z\mathbf{e}_z$, we can write

$$\delta n(\mathbf{r}) = -\mathbf{u}\cdot\frac{\partial}{\partial \mathbf{r}} n(\mathbf{r}) = Zn\cos\theta\delta(r-a).$$

We have neglected the oscillations of the density in the inner part of the particle due to shell effects, and also the extension of the electronic density outside of the particle (spillout effect).[2] Noting $V_{\mathrm{C}}(\mathbf{r},\mathbf{r}')$ the Coulomb electron-electron interaction, the change in the self-consistent potential due to the rigid shift (transition potential) is

$$\delta V(\mathbf{r}) = \int \mathrm{d}^3\mathbf{r}'\delta n(\mathbf{r}')V_{\mathrm{C}}(\mathbf{r},\mathbf{r}'). \tag{A1}$$

Using the multipolar decomposition of the Coulomb interaction, one obtains[3]

$$\delta V(\mathbf{r}) = Z\frac{4\pi n e^2}{3} d(\mathbf{r}), \tag{A2}$$

with

$$d(\mathbf{r}) = \begin{cases} z, & r \leqslant a, \\ \dfrac{za^3}{r^3}, & r > a. \end{cases} \tag{A3}$$

We notice that a displacement of the electron system leads to a dipolar field inside the nanoparticle, and that its magnitude decays as $1/r^2$ outside the particle.

If we now consider the case of a noble metal nanoparticle (where the d electrons are taken into account with the help of a dielectric constant ϵ_{d}) embedded in a matrix (of dielectric constant ϵ_{m}), the Coulomb interaction between electrons is given by[33]

$$V_{\rm C}(\mathbf{r},\mathbf{r}') = 4\pi e^2 \begin{cases} \dfrac{1}{\epsilon_{\rm d}} \displaystyle\sum_{lm} \frac{1}{2l+1} \left[\frac{r_<^l}{r_>^{l+1}} + \frac{r^l r'^l}{a^{2l+1}} \frac{(l+1)(\epsilon_{\rm d}-\epsilon_{\rm m})}{\epsilon_{\rm d} l + \epsilon_{\rm m}(l+1)} \right] Y_l^{m*}(\Omega) Y_l^m(\Omega'), & r,\ r' \leqslant a, \\ \displaystyle\sum_{lm} \frac{r_<^l}{r_>^{l+1}} \frac{Y_l^{m*}(\Omega) Y_l^m(\Omega')}{\epsilon_{\rm d} l + \epsilon_{\rm m}(l+1)}, & r_< \leqslant a,\ r_> > a, \\ \dfrac{1}{\epsilon_{\rm m}} \displaystyle\sum_{lm} \frac{1}{2l+1} \left[\frac{r_<^l}{r_>^{l+1}} + \frac{a^{2l+1}}{r^{l+1} r'^{l+1}} \frac{l(\epsilon_{\rm m}-\epsilon_{\rm d})}{\epsilon_{\rm d} l + \epsilon_{\rm m}(l+1)} \right] Y_l^{m*}(\Omega) Y_l^m(\Omega'), & r,\ r' > a, \end{cases}$$

where $r_< = \min(r, r')$, $r_> = \max(r, r')$, and Y_l^m are the spherical harmonics. Inserting this expression into Eq. (A1), we obtain the result of Eq. (A2) with the additional multiplying factor $3/(\epsilon_{\rm d} + 2\epsilon_{\rm m})$.

In both cases (with and without a dielectric mismatch), the expression (A2) can be written as $\delta V(\mathbf{r}) = Z m_{\rm e} \omega_{\rm M}^2 d(\mathbf{r})$. The only effect of the dielectric constants on the transition potential as compared to the free case is through the red-shift of the Mie frequency.

APPENDIX B: SEMICLASSICS WITH RADIAL SYMMETRY

Semiclassical expansions constitute a very useful tool in mesoscopic physics since they allow for an intuitive description of relatively complex systems. The spectral properties of metallic clusters[34] or the conductance fluctuations in the electronic transport through quantum dots[35] can be readily understood when the quantum observables are expressed in terms of an appropriate ensemble of classical trajectories.

In problems with radial symmetry, like the one we treat in this work, it is tempting to take advantage of the separability into radial and angular coordinates in order to reduce the dimensionality of the trajectories contributing to the semiclassical expansions. However there are technical difficulties introduced by the singularity at the origin of the centrifugal potential, and this is probably the reason why the radial symmetry is often not fully exploited in semiclassical expansions. On the other hand, the well-known Langer modification[36] is a prescription to avoid the above-mentioned difficulties and provides a route to the semiclassical quantization of spherically symmetric systems (which has been recently extended to higher orders[37]).

In this Appendix we start from the Langer modification in order to obtain the partial (or angular momentum dependent) density of states (DOS) $\varrho_l(\varepsilon)$ that we need in our evaluation of plasmon lifetimes. As a check of consistency, we verify in a few simple examples that when $\varrho_l(\varepsilon)$ is summed (in a semiclassical way) over l and m, we recover the well-known Berry-Tabor formula for the total DOS.[38,39]

1. Langer modification and partial density of states

For a central potential $V(r)$, the Schrödinger equation is separable into angular and radial parts. The wave function can be written as $\psi_{klm}(\mathbf{r}) = [u_{kl}(r)/r] Y_l^m(\Omega)$, where u_{kl} verifies

$$\left[-\frac{\hbar^2}{2m_{\rm e}} \frac{{\rm d}^2}{{\rm d}r^2} + \frac{\hbar^2 l(l+1)}{2m_{\rm e} r^2} + V(r) \right] u_{kl}(r) = \varepsilon_{kl} u_{kl}(r), \tag{B1}$$

with the condition $u_{kl}(0) = 0$. It is important to notice that the variable r is limited to positive values and that the centrifugal potential possesses a singularity at $r = 0$. This significant difference between Eq. (B1) and a standard one-dimensional Schrödinger equation prevents from a naive application of the Wentzel-Kramers-Brillouin (WKB) approximation to treat this radial problem. The change of variables $x = \ln r$ and $\chi_{kl}(x) = \exp(x/2) u_{kl}(r)$ results in a standard Schrödinger equation. Using the WKB approximation for χ_{kl} amounts to change the centrifugal potential in Eq. (B1) according to the Langer modification[36,40]

$$l(l+1) \Longrightarrow \left(l + \frac{1}{2} \right)^2 .$$

The resulting WKB quantization provides the exact spectrum for the hydrogen atom, as well as for the three-dimensional isotropic harmonic oscillator.

The same kind of considerations in two-dimensional systems with a circular symmetry leads to the following substitution in the centrifugal potential:[34,40]

$$\left(m - \frac{1}{4} \right)^2 \Longrightarrow m^2, \tag{B2}$$

which yields an exact WKB spectrum for the cases of the isotropic harmonic oscillator as well as for the hydrogen atom in two dimensions.

The semiclassical approximation provides a method to calculate the leading $\hbar$ contributions to the DOS in the limit of large quantum numbers, and decomposes the DOS into a smooth and an oscillating part. The smooth term is simply the Weyl contribution[34] and the oscillating term is given, in the case where the periodic orbits (POs) are not degenerated in action, by the Gutzwiller

trace formula[41] as a sum over the primitive periodic orbits (PPOs).

In the case of multidimensional integrable systems, the POs belonging to a torus of the phase space are degenerate, and the oscillating part of the DOS is given by the Berry-Tabor formula as a sum over rational tori.[39] In one-dimensional problems, or in the radial coordinate of a spherically symmetric case, the trajectories are not degenerate, and therefore the semiclassical approximation to the DOS at fixed angular momentum l is given by

$$\varrho_l(\varepsilon) = \varrho_l^0(\varepsilon) + \varrho_l^{\rm osc}(\varepsilon), \tag{B3}$$

with

$$\varrho_l^0(\varepsilon) = \frac{\tau_l(\varepsilon)}{2\pi\hbar},$$
$$\varrho_l^{\rm osc}(\varepsilon) = \frac{\tau_l(\varepsilon)}{\pi\hbar}\sum_{\tilde r=1}^{\infty}\cos\left[\tilde r\left(\frac{S_l(\varepsilon)}{\hbar} - \nu_{\rm c}\frac{\pi}{2} - \nu_{\rm r}\pi\right)\right],$$

where S_l and $\tau_l = \partial S_l/\partial\varepsilon$ are the action and period refering to the motion in the effective (l-dependent) radial potential; $\nu_{\rm c}$ ($\nu_{\rm r}$) is the number of classical turning points of the PPOs against the smooth (hard) walls.

2. Total density of states and Berry-Tabor formula for systems with radial symmetry

Using the selection rules for the plasmon decay, its lifetime can be expressed in terms of the partial DOS $\varrho_l(\varepsilon)$ whose semiclassical expression is given by Eq. (B3). It is then important to verify that the semiclassical sum over angular momenta (that we use throughout our calculations), when applied to $\varrho_l(\varepsilon)$, is able to reproduce the total DOS. Rather than working the most general case, we perform our test for three particular examples: the disk billiard (where the calculations are particularly simple), the three dimensional billiard (like the one we treat in the text), and the isotropic spherical harmonic oscillator (where the semiclassical spectrum coincides with the exact one).

a. Disk billiard

A disk billiard is defined by its radial potential

$$V(r) = \begin{cases} 0, & r < a, \\ \infty, & r \geqslant a, \end{cases} \tag{B4}$$

where a is the radius of the disk. The effective radial motion is governed by the potential $V_m^{\rm eff}(r) = \hbar^2 m^2/2m_{\rm e}r^2 + V(r)$, with m the z component of the angular momentum included according to Eq. (B2). The classical PPOs have $\nu_{\rm c} = \nu_{\rm r} = 1$ since there is one turning point at the (smooth) kinetic barrier and another at the (hard) wall for $r = a$. For a given energy ε we have $m_{\max} = (2m_{\rm e}\varepsilon)^{1/2}a/\hbar = (\varepsilon/\varepsilon_0)^{1/2} = ka$, with $\varepsilon_0 = \hbar^2/2m_{\rm e}a^2$.

The action and period of the PO with energy ε and angular momentum m are given by

$$S_m(\varepsilon) = 2\hbar\left[\sqrt{(ka)^2 - m^2} - m\arccos\left(\frac{m}{ka}\right)\right], \tag{B5a}$$
$$\tau_m(\varepsilon) = \frac{\hbar\sqrt{(ka)^2 - m^2}}{\varepsilon_0 (ka)^2}, \tag{B5b}$$

respectively. The smooth part of the DOS is

$$\varrho^0(\varepsilon) = \sum_{m=-m_{\max}}^{+m_{\max}} \varrho_m^0(\varepsilon) = \frac{1}{4\pi}\left(\frac{2m_{\rm e}}{\hbar^2}\right)\mathcal{A},$$

with $\mathcal{A} = \pi a^2$ being the disk area. We have replaced the sum by an integral and obtained the Weyl part of the DOS. For the oscillating part we make use of the Poisson summation rule and write

$$\varrho^{\rm osc}(\varepsilon) = \sum_{\tilde m=-\infty}^{+\infty}\sum_{\substack{\tilde r\geqslant 1\\ \sigma=\pm}}\int_0^{m_{\max}} {\rm d}m \frac{\tau_m(\varepsilon)}{2\pi\hbar}\, {\rm e}^{\sigma {\rm i}\phi_m^{\tilde m\tilde r}(\varepsilon)}$$

with the phase

$$\phi_m^{\tilde m\tilde r}(\varepsilon) = \tilde r\left[\frac{S_m(\varepsilon)}{\hbar} - \frac{3\pi}{2}\right] + 2\pi\tilde m m.$$

Consistently with the semiclassical expansions, we perform a stationary phase approximation. The stationary points are given by $\bar m = ka\cos\varphi_{\tilde r\tilde m}$, with $\varphi_{\tilde r\tilde m} = \pi\tilde m/\tilde r$ and the condition $\tilde r \geqslant 2\tilde m > 0$, which yield just the classical angular momenta of the POs labeled by the topological indices $(\tilde r, \tilde m)$. We then recover for the oscillating DOS the well-known result[38,39]

$$\varrho^{\rm osc}(\varepsilon) = \frac{1}{\varepsilon_0}\frac{1}{\sqrt{\pi ka}}\sum_{\tilde m=1}^{\infty}\sum_{\tilde r\geq 2\tilde m} f_{\tilde r\tilde m}\frac{\sin^{3/2}\varphi_{\tilde r\tilde m}}{\sqrt{\tilde r}}\cos\Phi_{\tilde r\tilde m},$$

where $f_{\tilde r\tilde m} = 1$ if $\tilde r = 2\tilde m$ and $f_{\tilde r\tilde m} = 2$ if $\tilde r > 2\tilde m$, $\Phi_{\tilde r\tilde m} = kL_{\tilde r\tilde m} - 3r\pi/2 + \pi/4$ and $L_{\tilde r\tilde m} = 2\tilde r a\sin\varphi_{\tilde r\tilde m}$ is the length of the orbit $(\tilde r, \tilde m)$.

We also notice that the quantization of the radial problem leads to the well-known Keller and Rubinow condition[42]

$$\sqrt{(ka)^2 - m^2} - m\arccos\left(\frac{m}{ka}\right) = \pi\left(n + \frac{3}{4}\right),$$

from which the Berry-Tabor formula can be readily obtained.

b. Spherical billiard

A spherical billiard is also defined by Eq. (B4), but in the three-dimensional case $V_l^{\rm eff}(r) = \hbar^2(l + 1/2)^2/2m_{\rm e}r^2 + V(r)$. For an energy ε, the maximum value of the angular momentum is given by $l_{\max} = ka - 1/2$. The action and the period of a trajectory with energy

ε and angular momentum l are the same as in the two-dimensional case up to a change of m by $l+1/2$ [Eqs. (B5)]. The total DOS is given by

$$\varrho(\varepsilon) = \sum_{l=0}^{l_{\max}} \sum_{m=-l}^{+l} \varrho_l(\varepsilon) = \sum_{l=0}^{l_{\max}} (2l+1)\varrho_l(\varepsilon).$$

For the smooth DOS, we find the first term of the Weyl expansion:[34]

$$\varrho^0(\varepsilon) = \frac{1}{4\pi^2}\left(\frac{2m_{\rm e}}{\hbar^2}\right)^{3/2}\sqrt{\varepsilon}\,\mathcal{V},$$

where $\mathcal{V} = 4\pi a^3/3$ is the volume of the sphere, and for the oscillating part

$$\varrho^{\rm osc}(\varepsilon) = \frac{1}{\varepsilon_0}\sqrt{\frac{ka}{\pi}} \times \sum_{\substack{\tilde{m}\geqslant 1 \\ \tilde{r}>2\tilde{m}}} (-1)^{\tilde{m}} \sin\left(2\varphi_{\tilde{r}\tilde{m}}\right)\sqrt{\frac{\sin\varphi_{\tilde{r}\tilde{m}}}{\tilde{r}}}\cos\Phi_{\tilde{r}\tilde{m}},$$

with the same notations as in Appendix B 2 a. We again recover the Berry and Tabor semiclassical DOS to leading order in $\hbar$,[38,39] as well as the quantization condition of Keller and Rubinow.[42]

c. *Isotropic spherical harmonic oscillator*

The isotropic harmonic oscillator in three dimensions is a nonbilliard integrable system and therefore the Berry-Tabor quantization is very difficult to implement. The radial approach that we develop clearly overcomes this difficulty. The effective potential is $V_l^{\rm eff}(r) = \hbar^2(l+1/2)^2/2m_{\rm e}r^2 + (1/2)m_{\rm e}\omega^2 r^2$, where ω is the pulsation of the harmonic confinement. At a given ε, we have $l_{\max} = -1/2 + \varepsilon/\hbar\omega$. The classical action is given by $S_l(\varepsilon) = \varepsilon\pi/\omega - \pi\hbar(l+1/2)$ and the period is $\tau = \pi/\omega$. Using Eq. (B3) with $\nu_{\rm c} = 2r$ and $\nu_{\rm r} = 0$ (no hard wall) gives the DOS at fixed orbital momentum.

For the smooth part of the DOS, the sum over l can be performed exactly, but to be consistent with the semiclassical approximation we have to take the limit $\varepsilon/\hbar\omega \gg 1$: $\varrho^0(\varepsilon) \simeq \varepsilon^2/2(\hbar\omega)^3$. Writing the Poisson summation rule for the oscillating part and performing a stationary phase approximation, we have the condition on topological indices $\tilde{r} = 2\tilde{m}$ and $\tilde{m} \geqslant 1$. Finally we obtain for the total DOS the trace formula

$$\varrho(\varepsilon) = \frac{\varepsilon^2}{2(\hbar\omega)^3}\left[1 + 2\sum_{\tilde{m}=1}^{\infty}(-1)^{\tilde{m}}\cos\left(2\pi\tilde{m}\frac{\varepsilon}{\hbar\omega}\right)\right],$$

which has to be compared with the exact trace formula given in Ref. 34, where the prefactor is shifted by the quantity $-1/8\hbar\omega$, negligible at the (high energy) semiclassical limit. One also notices that the WKB quantization rule yields the exact quantum spectrum of the harmonic oscillator: $\varepsilon_{nl} = \hbar\omega(2n+l+3/2)$.

We have demonstrated the usefulness of the radial decomposition for the semiclassical expansion of the DOS. Even in the case of degenerated classical periodic trajectories, one is able to find the semiclassical DOS by using the appropriate symmetry of the system, without requiring the action-angle quantization of Berry and Tabor.

3. Semiclassical dipole matrix element with spherical symmetry

In this Appendix we focus on the semiclassical evaluation of the dipole matrix element for the case of a spherically symmetric system, and extend the well-known result which relates in the one-dimensional case the dipole matrix element to the Fourier components of the classical motion of the particle.[43]

The spherical symmetry permits us to separate the dipole matrix element $\langle nlm|z|n'l'm'\rangle$ into two parts: an angular part given by Eq. (9) and a radial part

$$\mathcal{R}_{nn'}^{ll'} = \frac{\hbar^2}{m_{\rm e}(\varepsilon_{n'l'} - \varepsilon_{nl})}\int_0^\infty {\rm d}r\; u_{nl}(r)\frac{\rm d}{{\rm d}r}u_{n'l'}(r),$$

where the radial wave functions u_{nl} satisfy Eq. (B1) and we have used the commutation relation between the radial momentum and the Hamiltonian. Next we restrict ourselves to the classical region in the effective potential $V_l^{\rm eff}(r)$ between the two turning points (r_-, r_+) and use the WKB approximation to express the radial wave functions as

$$u_{nl}(r) = \frac{2\cos\left\{1/\hbar\int_{r_-}^{r}{\rm d}r'\sqrt{2m_{\rm e}\left[\varepsilon_{nl} - V_l^{\rm eff}(r')\right]} - \pi/4\right\}}{\sqrt{\tau_l}\left\{2m_{\rm e}\left[\varepsilon_{nl} - V_l^{\rm eff}(r)\right]/m_{\rm e}^2\right\}^{1/4}}.$$

We also assume that the radial potential is a smoothly varying function of the radial coordinate, that $l \simeq l'$ (this is justified because the selection rules dictate that $l' = l \pm 1$ and we are in the high energy limit) and that the energies involved in the dipole matrix element are sufficiently close to each other to satisfy

$$\varepsilon_{n'l'} - \varepsilon_{nl} \approx \frac{2\pi\hbar\Delta n}{\tau_l}, \tag{B6}$$

with $\Delta n = n' - n$.

With these approximations, changing the spatial coordinate r to the time t, we obtain, to leading order in $\hbar$

$$\mathcal{R}_{nn'}^{ll'} = \frac{2}{\tau_l}\int_0^{\tau_l/2}{\rm d}t\; r(t)\cos\left(2\pi\Delta n\frac{t}{\tau_l}\right), \tag{B7}$$

where $r(t)$ represents the classical trajectory in the effective potential. Thus we see that, as in the one-dimensional case, the dipole matrix element is related

to the Fourier transform of the trajectory of the classical motion.

As a check of consistency, we apply this semiclassical analysis to the hard-wall potential involved in our evaluation of the surface-plasmon lifetime. This analysis is only possible in the limit $\varepsilon_{\rm F} \gg \hbar\omega_{\rm M}$: The approximation of Eq. (B7) is valid if we assume that the energy of the particle is close to the one of the hole. This energy difference is, because of the conservation of energy appearing in the Fermi Golden Rule (6), simply $\hbar\omega_{\rm M}$.

At a given energy ε, the periodic trajectory in the effective potential is

$$r(t) = \sqrt{\frac{2\varepsilon}{m_{\rm e}} t^2 + \frac{\hbar^2 (l+1/2)^2}{2 m_{\rm e} \varepsilon}} \ , \ 0 \leqslant t \leqslant \frac{\tau_l}{2}.$$

Substituting this expression in Eq. (B7) and making the expansion in $1/\Delta n$ [proportional to $1/\hbar\omega_{\rm M}$, see Eq. (B6)], we obtain the leading order term

$$\mathcal{R}^{l_p l_h}_{k_p k_h} = \frac{2\hbar^2}{m_{\rm e} a} \frac{\varepsilon_p}{(\varepsilon_p - \varepsilon_h)^2}, \tag{B8}$$

which agrees with Eq. (11) in the limit $\varepsilon_p \approx \varepsilon_h$. We notice that this semiclassical dipole matrix element leads to the correct result for the smooth part Γ^0 of the single-plasmon linewidth in the limit $\xi = \hbar\omega_{\rm M}/\varepsilon_{\rm F} \to 0$ of Eq. (1).

APPENDIX C: FREQUENCY DEPENDENCE OF THE PLASMON LINEWIDTHS

In this Appendix, we present the frequency dependence of the single- and double-plasmon linewidths. In Fig. 5, we represent the function g (thick line) of $\xi = \hbar\omega_{\rm M}/\varepsilon_{\rm F}$ involved in the expression of the single-plasmon linewidth [see Eq. (1)], as well as in the first-order decay rate of the double plasmon ($\Gamma_{2\to 1}$). The function g is plotted after its analytical expression [Eqs. (62) and (63) in Ref. 13] and is a smoothly decreasing function with $\lim_{\xi\to\infty} g(\xi) = 0$.

The function h involved in the expression of the second-order double-plasmon linewidth (31) is defined by

$$h(\xi) = \int_{\max(1,2\xi)}^{1+2\xi} {\rm d}z \int_0^{z-2\xi} {\rm d}y \sqrt{z-y} \sqrt{z-y-2\xi} \times \left(\sqrt{\frac{z-y}{z}} - \sqrt{\frac{z-y-2\xi}{z-2\xi}} \right)^2$$

and has been approximately determined by integrating out the intermediate states i in the limit $k_{\rm F} a \gg 1$. The integral over the intermediate state energy has been performed by introducing cutoffs in order to avoid unphysical divergencies due to the fact that discrete single-particle levels have been replaced in our model by a continuum of states. When the remaining two-dimensional integral is evaluated numerically we obtain a smoothly increasing function of the parameter ξ, with $h(0) = 0$ as shown in Fig. 5. This function has the asymptotic limit $\lim_{\xi\to\infty} h(\xi) = \infty$. We see that when the double-plasmon state is too high in energy, the linewidth diverges to infinity and this resonance is no longer well-defined (the double-plasmon state has a lifetime equal to zero in this condition).

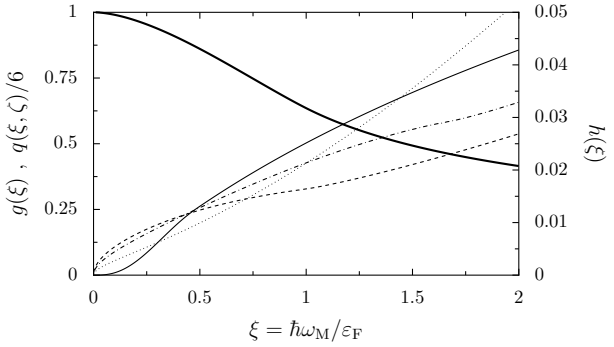

FIG. 5: Functions $g(\xi)$ (thick line), $h(\xi)$ (full line), and $q(\xi,\zeta)$. The function $q(\xi,\zeta)$ is represented as a function of ξ for $\zeta/\xi = 1$ (dashed line), 1.4 (dashed-dotted line), and 1.8 (dotted line).

The function q of the two variables ξ and $\zeta = W/\varepsilon_{\rm F}$ involved in our evaluation of the ionization rate via the double-plasmon state, Eq. (35), is defined as

$$q(\xi,\zeta) = \left(\frac{\xi}{2}\right)^6 \int_{\max(2\xi,1+\zeta)}^{1+2\xi} {\rm d}z \frac{(2z-1-\zeta)\sqrt{z-2\xi}}{z\sqrt{(z-\xi)(z-1-\zeta)}} \times \frac{1}{\left(\sqrt{z-\xi}-\sqrt{z-2\xi}\right)^4 \left(\sqrt{z}-\sqrt{z-\xi}\right)^2}. \tag{C1}$$

Since our approach is valid when $\hbar\omega_{\rm M} \leqslant W \leqslant 2\hbar\omega_{\rm M}$, the function q is defined for $\xi \leqslant \zeta \leqslant 2\xi$ and can be integrated numerically. The result is shown in Fig. 5. The function q is not very sensitive to the value of $\zeta/\xi = W/\hbar\omega_{\rm M}$ in the presented interval. However, it vanishes at the upper limit ($W = 2\hbar\omega_{\rm M}$), since in this case particle states cannot be in the continuum and $\Gamma_{\rm ion} = 0$.

* Electronic address: gweick@ipcms.u-strasbg.fr

[1] U. Kreibig and L. Genzel, Surf. Sci. **156**, 678 (1985); U. Kreibig and M. Vollmer, *Optical Properties of Metal Clusters* (Springer-Verlag, Berlin, 1995).

[2] W. A. de Heer, Rev. Mod. Phys. **65**, 611 (1993); M. Brack, *ibid.* **65**, 677 (1993).

[3] G. F. Bertsch and R. A. Broglia, *Oscillations in Finite Quantum Systems* (Cambridge University Press, Cambridge, 1994).

[4] J.-Y. Bigot, V. Halté, J.-C. Merle, and A. Daunois, Chem. Phys. **251**, 181 (2000).

[5] W. Ekardt, Phys. Rev. B **32**, 1961 (1985); E. K. U. Gross, J. F. Dobson, and M. Petersilka, in *Density Functional Theory II*, edited by R. F. Nalewajski, Topics in Current Chemistry Vol. **181** (Springer, Berlin, 1996).

[6] C. Bréchignac, P. Cahuzac, J. Leygnier, and A. Sarfati, Phys. Rev. Lett. **70**, 2036 (1993).

[7] K. P. Charlé, W. Schulze and B. Winter, Z. Physik D **12**, 471 (1989).

[8] T. Klar, M. Perner, S. Grosse, G. von Plessen, W. Spirkl, and J. Feldmann, Phys. Rev. Lett. **80**, 4249 (1998); F. Stietz, J. Bosbach, T. Wenzel, T. Vartanyan, A. Goldman, and F. Träger, *ibid.* **84**, 5644 (2000); C. Sönnichsen, T. Franzl, T. Wilk, G. von Plessen, and J. Feldmann, New J. Phys. **4**, 93.1 (2002).

[9] B. Lamprecht, J. R. Krenn, A. Leitner and F. R. Aussenegg, Appl. Phys. B **69**, 223 (1999).

[10] A. Arbouet, D. Christofilos, N. Del Fatti, F. Vallée, J. R. Huntzinger, L. Arnaud, P. Billaud, and M. Broyer, Phys. Rev. Lett. **93**, 127401 (2004).

[11] A. Kawabata and R. Kubo, J. Phys. Soc. Jpn. **21**, 1765 (1966).

[12] M. Barma and V. Subrahmanyam, J. Phys.: Condens. Matter **1**, 7681 (1989).

[13] C. Yannouleas and R. A. Broglia, Ann. Phys. (N.Y.) **217**, 105 (1992).

[14] C. Yannouleas, E. Vigezzi, and R. A. Broglia, Phys. Rev. B **47**, 9849 (1993).

[15] R. A. Molina, D. Weinmann, and R. A. Jalabert, Phys. Rev. B **65**, 155427 (2002); Eur. Phys. J. D **24**, 127 (2003).

[16] G. F. Bertsch, N. Van Giai, and N. V. Mau, Phys. Rev. A **61**, 033202 (2000).

[17] R. Schlipper, R. Kusche, B. von Issendorff, and H. Haberland, Phys. Rev. Lett. **80**, 1194 (1998); Appl. Phys. A: Mater. Sci. Process. **72**, 255 (2001).

[18] This is fulfilled for the nanoparticles we consider. The plasmon frequency is in the optical range and the corresponding wavelength is much larger than a.

[19] W. Kohn, Phys. Rev. **123**, 1242 (1961).

[20] L. Rodríguez-Sánchez, J. Rodríguez, C. Blanco, J. Rivas, and A. López-Quintela, J. Phys. Chem. B **109**, 1183 (2005).

[21] *Optical Properties of Solids*, edited by F. Abelès (North-Holland, Amsterdam, 1972).

[22] The discrepancy in Fig. 3(b) for $\epsilon_{\rm d} = \epsilon_{\rm m} = 1$ between Eq. (1) and the TDLDA is due to the uncertainty of the fitting procedure. For $r_{\rm s} = 3.93\ a_0$ (not shown), both points are in good agreement.

[23] M. Madjet, C. Guet, and W. R. Johnson, Phys. Rev. A **51**, 1327 (1995).

[24] M. C. Desjonquères and D. Spanjaard, *Concepts in Surface Physics*, 2nd ed. (Springer-Verlag, Berlin, 1996).

[25] J. Z. Gu and H. A. Weidenmüller, Nucl. Phys. A **690**, 382 (2001).

[26] J. Ritman, F.-D. Berg, W. Kühn, V. Metag, R. Novotny, M. Notheisen, P. Paul, M. Pfeiffer, O. Schwalb, H. Löhner, L. Venema, A. Gobbi, N. Hermann, K. D. Hildenbrand, J. Mösner, R. S. Simon, and K. Teh, Phys. Rev. Lett. **70**, 533 (1993).

[27] F. Catara, P. Chomaz, and N. Van Giai, Phys. Rev. B **48**, 18207 (1993).

[28] K. Hagino, Phys. Rev. B **60**, R2197 (1999).

[29] For $\hbar\omega_{\rm M} > W$, the ionization through a single-plasmon process is a relevant channel. See M. Koskinen and M. Manninen, Phys. Rev. B **54**, 14796 (1996).

[30] G. Weick, Ph.D. thesis, Université Louis Pasteur, unpublished.

[31] As a test of consistency, we checked that this approximation leads in the case of the single plasmon to a linewidth given by Eq. (1) for $\xi = 0$. For $\xi \neq 0$, we obtain a slightly different frequency-dependence, but with the same decreasing feature.

[32] M. Seidl and J. P. Perdew, Phys. Rev. B **50**, 5744 (1994).

[33] L. Serra, F. Garcías, J. Navarro, N. Barberán, M. Barranco, and M. Pi, Phys. Rev. B **46**, 9369 (1992).

[34] M. Brack and R. K. Bhaduri, *Semiclassical Physics* (Frontiers in Physics, Addison-Wesley, 1997).

[35] R. A. Jalabert, *The Semiclassical Tool in Mesoscopic Physics*, Proceedings of the International School of Physics "Enrico Fermi", Course CXLIII, edited by G. Casati, I. Guarneri and U. Smilansky (Soc. Italiana di Fisica, Bologna, 2000).

[36] R. E. Langer, Phys. Rev. **51**, 669 (1937).

[37] J. Hainz and H. Grabert, Phys. Rev. A **60**, 1698 (1999).

[38] R. Balian and C. Bloch, Ann. Phys. (N.Y.) **69**, 76 (1972).

[39] M. V. Berry and M. Tabor, Proc. R. Soc. London, Ser. A **349**, 101 (1976); J. Phys. A **10**, 371 (1977).

[40] M. V. Berry and K. E. Mount, Rep. Prog. Phys. **35**, 315 (1972).

[41] M. C. Gutzwiller, *Chaos in Classical and Quantum Mechanics* (Springer-Verlag, Berlin, 1990).

[42] J. B. Keller and S. I. Rubinow, Ann. Phys. (N.Y.) **9**, 24 (1960).

[43] See, e.g., L. D. Landau and E. M. Lifshitz, *Quantum Mechanics*, Sec. 48 (Pergamon, New York, 1959).